Cover Letter
to the manuscript entitled

Judd-Ofelt analysis and stimulated-emission cross-sections for highly doped (38 at.%) Er:YSGG laser crystal

Authors:

P.A. Loiko, E. A. Arbabzadah, M. J. Damzen, X. Mateos, E.B. Dunina, A.A. Kornienko, A.S. Yasukevich, N.A. Skoptsov and K.V. Yumashev

The author to whom correspondence should be addressed:
Dr. Pavel Loiko,
Center for Optical Materials and Technologies,
Belarusian National Technical University,
220013 Belarus, Minsk, 65/17 Nezavisimosti Ave.,
Tel. +375(17)2939188, Fax. +375(17)2926286,
e-mail: kinetic@tut.by

In the present paper, we report on a comprehensive spectroscopic study of yttrium scandium gallium garnet, YSGG, highly-doped (38 at.%) with Er^{3+} ions. Main focus of this work is the determination of stimulated-emission cross-sections spectra for ~1.5 μm ($^4I_{13/2} \rightarrow {}^4I_{15/2}$) and ~3 μm ($^4I_{11/2} \rightarrow {}^4I_{13/2}$) transitions of Er^{3+} ions, *for the first time, to the best of our knowledge*. Absorption cross-sections spectra are also determined. This information is crucial for development of novel near-IR and mid-IR erbium lasers. To determine radiative lifetimes of the excited states of Er^{3+} ions, we involve Judd-Ofelt theory modified for systems with an intermediate configuration interaction. Up-conversion is also studied for this crystal. Finally, laser operation with Er:YSGG crystal at ~3 μm is achieved.

We confirm that the manuscript is the *authors' original work*; it has not been published and it has not been submitted simultaneously elsewhere. We also confirm that all authors have checked the manuscript and have agreed to the submission.

Dear Editor,

Thank you for considering our manuscript for publication in Journal of Luminescence and for permitting us this opportunity to respond to the reviewers' comments.
We welcome the comments from the reviewers and have complied with all of the comments.

A detailed list of the corrections follows.

Reviewer #1

The authors have answered satisfactorily all my requirements. There is only one more thing I have not noticed up to now and I really have to check:

1. Page 3: The authors do not specify explicitly whether the contributions of the magnetic dipole to the experimental oscillator strengths were subtracted before fitting the data with the Judd-Ofelt model. If they were subtracted, please specify this fact in the paper. If this is not the case, the calculations should be corrected.
Yes, we have subtracted MD contributions to the experimental oscillator strengths prior to the Judd-Ofelt modeling. Now this is specified in the text (page 3):

Prior to the fitting of experimental oscillator strengths with the J-O model, MD contributions were subtracted from the f_{exp} *values.*

Judd-Ofelt analysis and stimulated-emission cross-sections for highly doped (38 at.%) Er:YSGG laser crystal

P.A. Loiko[1,*], E. A. Arbabzadah[2], M. J. Damzen[2],
X. Mateos[3], E.B. Dunina[4], A.A. Kornienko[4],
A.S. Yasukevich[1], N.A. Skoptsov[1] and K.V. Yumashev[1]

[1] *Center for Optical Materials and Technologies, Belarusian National Technical University, 65/17 Nezavisimosti Ave., Minsk 220013, Belarus*
[2] *Photonics, The Blackett Laboratory, Imperial College London, London SW7 2BW, UK*
[3] *Física i Cristal·lografia de Materials i Nanomaterials (FiCMA-FiCNA), Universitat Rovira i Virgili (URV), Campus Sescelades, c/ Marcel·lí Domingo, s/n., Tarragona, Spain E-43007*
[4] *Vitebsk State Technological University, 72 Moskovskaya Ave., Vitebsk, Belarus 210035*

**Corresponding author e-mail: kinetic@tut.by*
Tel. +375(17)2939188, Fax. +375(17)2926286

Abstract Stimulated-emission cross-section spectra are determined for the ~1.5 μm and 3 μm transitions of Er^{3+} ions in YSGG crystal. For the $^4I_{11/2} \rightarrow {}^4I_{13/2}$ channel, the maximum stimulated-emission cross-section σ_{SE} is 0.43×10^{-20} cm^2 at 2797.1 nm. For the $^4I_{13/2} \rightarrow {}^4I_{15/2}$ channel, $\sigma_{SE} = 1.20\times10^{-20}$ cm^2 at 1532.8 nm. Due to the reabsorption loss, laser operation is expected at ~1644 nm. Radiative lifetimes of all excited states of the Er^{3+} ion from $^4I_{13/2}$ to $^2H_{9/2}$ and probabilities of radiative transitions from these states are determined using the Judd-Ofelt theory. Radiative lifetimes of the $^4I_{13/2}$ and $^4I_{11/2}$ excited states for Er^{3+} ions in YSGG are 7.73 ms and 9.75 ms, respectively. Non-radiative decay is analyzed for lower excited-states of Er^{3+} ions in YSGG.

Keywords: erbium ions; gallium garnets; Judd-Ofelt analysis; stumulated emission

1. Introduction

Erbium-doped garnets are widely used as laser crystals for the generation of ~1.5 and 3 μm radiation [1-4]. The 3 μm transition of Erbium doped lasers falls at a peak in the water absorption spectrum making laser sources at this wavelength extremely useful in medicine and dentistry [5,6]. A difficulty associated with this laser transition is that the lower laser level ($^4I_{13/2}$) has a longer lifetime than the upper laser level ($^4I_{11/2}$), which would usually result in self terminating behavior [7-10]. However, with highly doped Erbium crystals this effect can be counteracted via energy transfer upconversion (ETU) processes which recycle population from the lower laser level back to the upper laser level (and are stronger at higher doping levels when the Er^{3+}–Er^{3+} inter-ionic distance is less) [7-10]. This mechanism is shown in Fig. 1 (labeled W_{11}) which is an energy level diagram for the system.

For successful laser construction and theoretical modeling of ~3 μm laser systems it is necessary to have accurate spectroscopic data on highly doped Erbium crystals. The majority of 3 μm laser studies on Erbium doped garnets has been undertaken using Er:YAG, but an interesting competitor for this material is Er:$Y_3Sc_2Ga_3O_{12}$ (Er:YSGG) [11,12]. This crystal has a significantly longer upper laser level lifetime for the ~3 μm transition, $^4I_{11/2}$, compared to Er:YAG (1.3 ms vs. 120 μs [2]), providing better energy storage potential which could translate into superior Q-switched performance. Moreover the shorter lower laser level lifetime of Er:YSGG compared to Er:YAG [2] could prove advantageous in reducing the likelihood of self-termination of the 3 μm transition. Spectroscopic properties of Er,Cr:YSGG were studied in [13,14]. Previous papers on Er:YSGG focused on structure of energy-levels of Er^{3+} ions [15], Judd-Ofelt modeling [16,17] and up- conversion luminescence [18,19]. However, some relevant spectroscopic parameters of the Er:YSGG material are still not well known, specifically the stimulated emission cross section for both the ~1.5 and 3 μm transition.

In this work, a detailed spectroscopic study of a highly doped 38 at.% Er:YSGG crystal is undertaken. Absorption and luminescence spectra are presented and stimulated emission cross sections are calculated for the ~1.5 and 3 μm laser transitions. The radiative lifetimes of the relevant excited states of the Erbium system are calculated using the conventional Judd-Ofelt (J–O) theory. Furthermore, the luminescence branching ratios, absorption oscillator strengths and probabilities of spontaneous radiative transitions are determined.

2. Experimental

The studied crystal was $Y_3Sc_2Ga_3O_{12}$ (YSGG) doped with 38 at.% Er. The Er concentration, N_{Er}, determined with Electron Probe MicroAnalysis (EPMA) was 48.2×10^{20} at/cm^3. Such a high Er content was selected as it corresponded to the typical doping levels (30...50 at.%) for Er:YSGG active elements used in ~3 μm lasers reported so far [2,11,12]. In addition, we aimed to study the influence of high doping level on the spectroscopic parameters of Er^{3+} ions. Indeed, as the ionic radius of six-fold oxygen-coordinated Y^{3+} ion (0.90 Å) is slightly larger than that of Er^{3+} ion (0.89 Å), high-level crystal doping can induce slight variation of the crystal structure and, hence, f-f transition intensities. For instance, this effect was observed for 0.5–29 at.% Er-doped YAG crystals [20].

Optical absorption spectra of Er:YSGG were measured with a Varian CARY 5000 spectrophotometer at room-temperature (RT, ~293 K). The spectral bandwidth (SBW) was ~0.02 nm. To avoid saturation of the detector, the sample used for absorption measurements was a thin (thickness: 100 μm) polished plate.

Photoluminescence (PL) of Er^{3+} ions was excited by the focused output of a 962 nm InGaAs laser diode (the maximum power density on the sample was ~1 kW/cm^2). The PL was collected in the direction perpendicular to the excitation direction by a wide-aperture lens. The spectrum was registered by means of a lock-in amplifier, monochromator MDR-23 (SBW ~0.2 nm) and sensitive Hamamatsu C5460-01 (0.4–0.9 μm) and G5851 (0.9–1.7 μm) photodetectors. The monochomator was calibrated with Xe lamp. The emission of the Er^{3+} ions at ~3 μm was detected with a compact

Fourier transform infrared spectrometer, FT-IR Rocket from Arcoptix. As an excitation source, Ti:Sapphire laser tuned to ~962 nm was used.

For the luminescence decay measurements, an optical parametric oscillator Lotis TII LT-2214 tuned to 545, 650, 800, 960 or 1480 nm was used as the excitation source; the duration of the excitation pulse was ~20 ns. The PL was collected by a wide-aperture lens and re-imaged to the input slit of the monochromator MDR-12 (SBW ~1 nm), before detection by a fast Hamamatsu C5460 or G5851 photodetector (response time, 40 ns) and 500 MHz Textronix TDS-3052B digital oscilloscope.

3. Results and discussion

The absorption spectrum of the Er:YSGG crystal is shown in Fig. 2. The absorption band related to the $^4I_{15/2} \rightarrow {}^4I_{11/2}$ transition, used for pumping of Er:YSGG crystals with InGaAs laser diodes, contains three intense peaks centered at 962.5, 965.8 and 968.8 nm. The corresponding absorption cross-section, σ_{abs}, is ~0.46×10^{-20} cm^2. Full width at half maximum (FWHM) for these peaks is relatively small, <1.5 nm. For the band related to the $^4I_{15/2} \rightarrow {}^4I_{13/2}$ transition, typically used for the resonant (inband) pumping of Er^{3+} lasers, the maximum σ_{abs} value is 1.02×10^{-20} cm^2 at 1532.6 nm. The spectral features determined for 38 at.% Er:YSGG crystal are similar to one reported in [16,17] for the same crystal with a lower Er doping level.

Absorption oscillator strengths for Er^{3+} ions were calculated directly from the measured absorption spectrum $\alpha(\lambda)$:

$$f_{\exp} = \frac{m_e c^2}{\pi e^2 N_{Er} \bar{\lambda}^2} \int \alpha(\lambda) d\lambda \,, \tag{1}$$

where $\bar{\lambda}$ is the coordinate of a "center of gravity" of the selected absorption band (mean wavelength), N_{Er} is the concentration of Er^{3+} ions, m_e and e are the electron mass and charge, respectively; the integration is performed over the absorption band.

In addition, absorption oscillator strengths were calculated from the line strength S(JJ') modeled within the conventional Judd-Ofelt (J–O) theory [21,22]:

$$S_{ED}(JJ') = \sum_k e^2 \Omega_k \, |\langle \gamma J | U^k | \gamma' J' \rangle|^2 \,. \tag{2}$$

Here, the summation is performed for k = 2, 4, 6; $|\langle \gamma J|U^k|\gamma' J'\rangle|^2$ is the square of reduced matrix element of the unit matrix U^k, E_J and $E_{J'}$ are the energies of γJ and $\gamma' J'$ multiplets, {Ω_2, Ω_4 and Ω_6} are the intensity (J–O) parameters. An expression for the calculation of f values from the corresponding line strengths is:

$$f_{ED} = \frac{8\pi^2 m_e c}{3(2J+1)\bar{\lambda} h e^2} \frac{(n^2+2)^2}{9n} S_{ED}(JJ') \,, \tag{3}$$

where n is the crystal refractive index [23] at the wavelength of $\bar{\lambda}$. J-O theory allows for a calculation of the line strengths for electric-dipole (ED) transitions. The contribution of magnetic-dipole (MD) transitions with J–J' =0,±1 was calculated separately using the Russell- Saunders approximation on wave functions of Er^{3+} ions under the assumption of a free-ion. Total calculated oscillator strengths were then $f_{calc} = f_{ED} + f_{MD}$. Prior to the fitting of experimental oscillator strengths with the J-O model, MD contributions were subtracted from the f_{exp} values.

The wave functions in the intermediate coupling scheme (ICS) corresponding to the states (energy levels) of the rare-earth ions are linear combinations of wave functions in the Russell-Saunders approximation (the L-S coupling scheme). The energy levels are designated usually by means of one or more L-S wave functions which contribute mainly to this linear combination. For designating of high-lying excited-states of Er^{3+} (see Fig. 1), we used this system. This means that the L-S wave functions $(^2G,{}^4F,{}^2H)_{9/2}$, $(^2P,{}^2D,{}^4F)_{3/2}$ and $(^2H,{}^2G)_{9/2}$ contribute mainly to the ICS wave function of Er^{3+} with energy level of ~24550 cm^{-1}, 31600 cm^{-1} and 36550 cm^{-1}, respectively.

Results on the experimental and calculated absorption oscillator strengths of Er^{3+} ions are presented in Table 1. For J–O theory, the obtained parameters are Ω_2 =2.22, Ω_4 =1.50 and Ω_6 =0.46 [10^-

^{20} cm^2]. In Table 2, we compared obtained J–O parameters with the ones reported previously for Er:YSGG [16,17] and different Er-doped crystals [24-28]. In addition, spectroscopy quality factors, $X_{2/6} = \Omega_2/\Omega_6$ and $X_{4/6} = \Omega_4/\Omega_6$, introduced by Kaminski [24], are calculated. They are used to estimate the potential of active materials for laser operation as they are linked to the luminescence branching ratios. For Er:YSGG, $X_{2/6} = 4.82$ and $X_{4/6} = 3.26$ that agrees with the range determined by Kaminski [24], Table 2. J–O parameters obtained in the present paper for 38 at.% Er:YSGG are different from the ones reported by Su et al. for 30 at.% Er:YSGG [16], Ω_2 =0.23, Ω_4 =0.86 and Ω_6 =0.37 and by Sardar et al. for 1 at.% Er:YSGG [17], Ω_2 =0.92, Ω_4 =0.48 and Ω_6 =0.87 [10^{-20} cm^2]. This is partially referred to the difference in Er concentration. Indeed, J–O parameters are sensitive to the intensities of hypersensitive Er^{3+} transitions [24] which are in turn affected by the crystal field.

It is well known that the excited configurations can affect the Stark splitting of the multiplets [29] as well as transition intensities [30]. These configurations have different influence on the lower and higher lying multiplets. This is mainly related to the energy gap between the multiplet and excited configuration. Within the J–O theory, excited configurations are considered to be completely degenerated and thus the above mentioned influence is not taken into account. The use of J–O theory for the description of transition intensities for Er^{3+} doped materials is typically successful [24–28]. This is due to the fact that multiplets of Er^{3+} ion are strongly "mixed" by the crystalline field and the difference in the action of excited configurations on different multiplets is near negligible. Indeed, the J-O theory allowed us to obtain low root-mean-square (rms) deviation between the experimental and calculated *f* values (rms dev. = 0.245).

PL spectra of the Er:YSGG crystal are shown in Fig. 3 (for excitation to the $^4I_{11/2}$ state by 962 nm radiation). Near-IR emissions at 0.95–1.05, 1.45–1.66 and 2.6–2.95 μm correspond to the transitions $^4I_{11/2} \rightarrow {}^4I_{15/2}$, $^4I_{13/2} \rightarrow {}^4I_{15/2}$ and $^4I_{11/2} \rightarrow {}^4I_{13/2}$, respectively. All visible emissions are due to up-conversion luminescence (UCL). The red emission band spanning from 640 to 690 nm and related to the transition $^4F_{9/2} \rightarrow {}^4I_{15/2}$ dominates in this spectrum. Green UCL (510–570 nm) from the closely located and thermalized states, $^2H_{11/2}$ and $^4S_{3/2}$, is much weaker. The ratio of the integrated intensities of these bands (R/G) is 3.1. Near-IR UCL at 780–870 nm is due to the $^4I_{9/2} \rightarrow {}^4I_{15/2}$ and $^4S_{3/2} \rightarrow {}^4I_{13/2}$ transitions. In the blue-violet region, very weak emissions at ~ 415 and 450 nm occur from the higher-lying $^2H_{9/2}$ and $^4F_{3/2}$+$^4F_{5/2}$ excited states, respectively.

In Fig. 4, log-log plots for the UCL intensity, I_{UCL}, vs. the excitation power density *W* are shown. UCL is a non-linear process, so typically $I_{UCL} \sim W^n$ (the so-called power law). The parameter *n* indicates the number of pump photons involved in the UCL mechanism. On a log-log scale, *n* corresponds to the slope of the above mentioned dependence. First we consider the case of low power densities (< 0.2 kW/cm^2). For green emissions that occur from the $^2H_{11/2}$ and $^4S_{3/2}$ states, *n* = 1.8 (542 nm) and 2.0 (557 nm) which means that two pump photons are required to populate the above mentioned states. A pump wavelength of ~962 nm corresponds to the ground-state absorption (GSA) $^4I_{15/2} \rightarrow {}^4I_{11/2}$. Further excitation is typically due to an excited state absorption (ESA) $^4I_{11/2} \rightarrow {}^4F_{7/2}$ or energy-transfer up-conversion (ETU) for adjacent Er^{3+} ions, $^4I_{11/2}$+ $^4I_{11/2} \rightarrow {}^4I_{15/2}$ + $^4F_{7/2}$. Taking into account fast non-radiative relaxation from the $^4F_{7/2}$ state, both $^2H_{11/2}$ and $^4S_{3/2}$ states are normally populated in a scheme that requires 2 pump photons that is in agreement with Fig. 4(a). For near-IR UCL at 857 nm, also occurring from the $^4S_{3/2}$ state, *n* = 1.9.

For red emission at 672 nm, *n* = 2.0. Population of the $^4F_{9/2}$ state, which is responsible for this emission, normally occurs in three steps. These are GSA, followed by a non-radiative relaxation to the intermediate $^4I_{13/2}$ level and second intense ESA channel $^4I_{13/2} \rightarrow {}^4F_{9/2}$. For crystals with a high Er content like in our case, there is an additional mechanism that allows for further enhancement of the excitation efficiency, namely cross-relaxation (CR). First intense CR scheme is $^4F_{7/2}$ + $^4I_{15/2} \rightarrow {}^4F_{9/2}$ + $^4I_{13/2}$ that raises red UCL. Second relevant CR scheme is $^4S_{3/2}$,$^2H_{11/2}$ + $^4I_{15/2} \rightarrow {}^4I_{9/2}$ + $^4I_{13/2}$ that depopulates thermalized $^4S_{3/2}$,$^2H_{11/2}$ states responsible for green emission. Increase of Er doping leads to a decrease of average inter-ionic distances and, hence, to a fast enhancement of the CR efficiency. In contrast, ESA process is not significantly affected by Er doping level. Thus, red UCL is

enhanced much stronger as compared with the green UCL from the thermalized $^2H_{11/2}$ + $^4S_{3/2}$ states that results in R/G ratio being > 1 for highly Er-doped crystals. Indeed, for 38 at. % Er:YSGG, R/G = 3.1 as mentioned above.

The reduced value of n for red UCL at high excitation power densities >0.2 kW/cm^2 (n ~1.1) is related to the competition of a linear decay (near-IR luminescence around 1.54 μm from the $^4I_{13/2}$ state) and upconversion itself (due to ESA from the $^4I_{13/2}$ state) in the depletion of the intermediate excited state, $^4I_{13/2}$. It was shown [31] that for strong UCL, n is typically <2 and can even approach 1. This prediction agrees with our results shown in Fig. 4. Similar behavior is observed for green and near-IR UCL.

Using the parameters presented in Table 2, we calculated line strengths $S_{ED}(JJ')$ for spontaneous radiative transitions from all excited states of the Er^{3+} ion from $^4I_{13/2}$ to $^2H_{9/2}$. On the basis of $S_{ED}(JJ')$ values, the corresponding probabilities of these transitions $A_{ED}(JJ')$ were determined as:

$$A_{ED}(JJ') = \frac{64\pi^4}{3h(2J+1)\bar{\lambda}^3} n\left(\frac{n^2+2}{3}\right)^2 S_{ED}(JJ') . \quad (4)$$

The total probabilities, $A(JJ') = A_{ED}(JJ') + A_{MD}(JJ')$, were then determined by adding MD contributions determined separately. Radiative lifetimes of the excited-states τ_{rad} and luminescence branching ratios $B(JJ')$ were then determined as:

$$\tau_{rad} = \frac{1}{\sum_{J'} A(JJ')} , \quad (5a)$$

$$B(JJ') = \frac{A(JJ')}{\sum_{J'} A(JJ')} . \quad (5b)$$

Luminescence branching ratios $B(JJ')$ for spontaneous radiative transitions from the $^4I_{13/2}$...$^2H_{9/2}$ states of Er^{3+} ions in YSGG determined with the J–O theory are shown in Table 3. For transitions from the $^4I_{11/2}$ state that is the upper-laser level for ~3 μm Erbium lasers, $B(^4I_{11/2} \rightarrow {}^4I_{15/2})$ = 74.6% and B ($^4I_{11/2} \rightarrow {}^4I_{13/2}$) =25.4%. In Table 4, we compared these values with the ones reported previously for Er:YSGG and different well-known Er-doped laser materials. The values calculated by us agree well with the ones reported for 30 at.% Er:YSGG in [16], namely 72.6% and 27.4%, respectively. They are also in agreement with ones presented for cubic garnets, Er:YAG, LuAG [24], GGG and GSGG [32].

Radiative lifetimes τ_{rad} for the $^4I_{13/2}$...$^2H_{9/2}$ excited-states of Er^{3+} ions in YSGG crystal are summarized in Table 5. Relatively good agreement of all τ_{rad} values is observed with the previous report for 30 at.% Er:YSGG [16]. For $^4I_{13/2}$ and $^4I_{11/2}$ states which are interesting for laser applications, τ_{rad} is 7.73 and 9.75 ms, respectively (as determined with the J–O theory). This is close to the result of [16] also obtained with the J–O theory, namely 6.62 and 8.87 ms, respectively. In Table 6, we compared radiative lifetimes of the $^4I_{13/2}$ and $^4I_{11/2}$ states for different Er^{3+}-doped crystals reported so far. A relatively good agreement of results for the $^4I_{13/2}$ state is observed. In contrast, for the $^4I_{11/2}$ state, the value of τ_{rad} for the Er:YSGG crystal is longer than ones determined for cubic Er-doped garnets (5–8 ms) [17,24] that highlights its potential for 3 μm laser operation.

The knowledge of radiative lifetimes τ_{rad} for the $^4I_{13/2}$ and $^4I_{11/2}$ states allows for determination of stimulated-emission cross-sections, σ_{SE}, for laser-active transitions $^4I_{13/2} \rightarrow {}^4I_{15/2}$ (lasing at ~1.5 μm) and $^4I_{11/2} \rightarrow {}^4I_{13/2}$ (at ~3 μm). In both cases, the Füchtbauer–Ladenburg (F-L) equation [35] was used:

$$\sigma_{SE}(\lambda) = \frac{\lambda^5}{8\pi n^2 \tau_{rad} c} \frac{3W(\lambda)}{\int \lambda W(\lambda) d\lambda} . \quad (6)$$

Here $W(\lambda)$ is the measured spectral power density of luminescence. In addition, for the $^4I_{13/2} \rightarrow {}^4I_{15/2}$ transition, we used the reciprocity method:

$$\sigma_{SE}(\lambda) = \sigma_{abs}(\lambda) \frac{Z_1}{Z_2} \exp\left(-\frac{hc/\lambda - E_{ZL}}{kT}\right) , \quad (7)$$

where Z_1 and Z_2 are the lower and upper manifold partition functions, respectively, E_{ZL} is the energy corresponding to the zero phonon line, k is the Boltzmann constant and T is the crystal temperature (room-temperature). Partition functions are determined as:

$$Z_m = \sum_k g_k^m \exp(-E_k^m/kT), \tag{8}$$

where m = 1, 2; $g^m{}_k$ is the degeneration of the sublevel having the number k and the energy $E^m{}_k$ measured from the lower sublevel of the corresponding multiplet. The energies of sublevels for the $^4I_{13/2}$ and $^4I_{15/2}$ multiplets for Er:YSGG crystal were taken from [15]. Calculation of σ_{SE} with the reciprocity method is beneficial as it does not require the information about the radiative lifetime τ_{rad} of the emitting state as well as direct measurement of the emission spectrum that can be affected by the reabsorption loss. There exists third possibility for the calculation of σ_{SE} values, the so-called modified reciprocity method [36]:

$$\sigma_{SE}(\lambda) = \frac{3\exp(-hc/(kT\lambda))}{8\pi n^2 \tau_{rad} c \int \lambda^{-4} \sigma_{abs}(\lambda) \exp(-hc/(kT\lambda)) d\lambda} \sigma_{abs}(\lambda). \tag{9}$$

Modified reciprocity method does not refer to the emission spectrum $W(\lambda)$ but it requires the data about τ_{rad} value. Thus, a simultaneous use of Eqs. (7) and (9) can result in an estimation of the radiative lifetime of the emitting state that is the $^4I_{13/2}$ state in our case.

The results for σ_{SE} are shown in Fig. 5. For the $^4I_{13/2} \rightarrow {}^4I_{15/2}$ transition, the use of reciprocity method corresponds to a better resolution of spectral features as compared with the F–L equation, partially referred to a better spectral resolution used in the absorption measurements and partially to the reabsorption losses that are strong for highly doped 38 at.% Er:YSGG crystals. The maximum stimulated-emission cross-section σ_{SE} is 1.20×10^{-20} cm^2 at 1532.8 nm. Estimation of the radiative lifetime τ_{rad} of the $^4I_{13/2}$ state with the modified reciprocity method yields the value of 5.5±0.5 ms that is shorter than one determined from the J–O modeling, 7.73 ms. This effect was previously observed in [32]. It can be explained as following. In the J–O theory, it is assumed that all the crystal field levels of each multiplet are equally populated. For the case of Er:YSGG crystal, the $^4I_{15/2}$ ground state is split into two groups of four levels separated by ~400 cm^{-1} [15]. Thus, the transitions from the four lower $^4I_{15/2}$ sub-levels to the $^4I_{11/2}$ and $^4I_{13/2}$ states are much stronger than they are from the upper four sub-levels. Since the lower group of levels is predominantly populated at room temperature, this splitting leads to an enhancement of the observed oscillator strength and therefore slight underestimate of the Judd-Ofelt radiative lifetime.

For laser applications, a useful parameter is also the gain cross-section, σ_g:

$$\sigma_g(\lambda) = \beta\sigma_{SE}(\lambda) - (1-\beta)\sigma_{abs}(\lambda), \tag{10}$$

where β is the inversion ratio, $\beta = N_2/N_0$ where N_2 and N_0 are the numbers of ions in the upper laser level and overall number of ions, respectively. The gain spectra for the Er:YSGG crystal for β <0.5 are shown in Fig. 5(b). In accordance with this plot, the dominant wavelength in the Er:YSGG laser working on the $^4I_{13/2} \rightarrow {}^4I_{15/2}$ transition will be at ~1644 nm. This is in agreement with the report on an Er:YSGG inband-pumped laser emitting at 1643 nm [37]. For real ~1.5 μm laser applications, concentration of Er^{3+} ions of <1 at.% should be selected to avoid the detrimental influence of strong up-conversion.

For the $^4I_{11/2} \rightarrow {}^4I_{13/2}$ channel, the maximum stimulated-emission cross-section is 0.43×10^{-20} cm^2 at 2797.1 nm, Fig. 5(c). This emission channel is free of reabsorption losses, so one can expect generation at this wavelength in an Er:YSGG laser.

Peak stimulated-emission cross-sections σ_{SE} for the $^4I_{13/2} \rightarrow {}^4I_{15/2}$ and $^4I_{11/2} \rightarrow {}^4I_{13/2}$ transitions of Er^{3+} ions for Er:YSGG and several Er^{3+}-doped crystals are compared in Table 7. It should be noted that σ_{SE} *spectrum* was never reported for the $^4I_{11/2} \rightarrow {}^4I_{13/2}$ transition of Er^{3+} ions in the YSGG crystal. Previously for the calculation of peak σ_{SE} value corresponding to this transition, lifetime of the $^4I_{11/2}$ upper laser level reported by Dinerman, τ_{exp}=3.4 ms [2], was used. This led to the overestimation of the σ_{SE} value that was typically considered to be ~2.8×10^{-20} cm^2. However, as in [2] τ_{exp} was determined directly from the PL decay curves for a highly-doped (30 at.% Er) crystal, it was much shorter

than the radiative lifetime, namely 9.75 ms as determined in the present paper from the J–O modeling. Similar situation for different Er-doped crystals is addressed in details in [32]. For the $^4I_{13/2} \rightarrow {}^4I_{15/2}$ transition, stimulated-emission and gain cross-sections spectra were also not reported for Er:YSGG crystal. However, the obtained peak σ_{SE} values for this transition are in accordance with the ones reported previously for different Er-doped materials, see Table 7.

The measured decay curves for the luminescence from the five lowest excited-states of Er^{3+} ions in YSGG are shown in Fig. 6 ($^4S_{3/2}$ and $^2H_{11/2}$ levels are treated as a single, thermally coupled level). Relatively high Er concentration should lead to significant concentration quenching and a high rate of non-radiative relaxation in the Er:YSGG crystal. Thus, shortening of the measured lifetime, τ_{exp}, as compared with the radiative one, τ_{rad}, is expected for all excited-states of Er^{3+} ions. The measured decay times τ_{exp} of the luminescence from the $^4I_{13/2}$ and $^4I_{11/2}$ states are 2.24 and 1.3 ms, respectively (compare with the corresponding radiative lifetimes, 7.73 and 9.75 ms as determined from the J–O modeling). The value of $\tau_{exp}(^4I_{13/2})$ obtained in the present paper for 38 at.% Er:YSGG crystal is shorter than the value reported in [2] for 30 at.% Er doped crystal, namely 3.2 ms. For the $^4I_{9/2} - {}^2H_{11/2}$ states, the measured lifetimes are on the order of a few μs (cf. Table 5). By comparing τ_{rad} for the $^4F_{9/2}$ state (responsible for red emission) and the thermalized $^4S_{3/2}+{}^2H_{11/2}$ states (responsible for green UCL), the prevalence of red emission in the UCL can be explained. Indeed, $\tau_{rad}(F_{9/2}) = 10.2$ μs which is nearly 25 times longer than for the $^4S_{3/2}$ and $^2H_{11/2}$ states. In addition, the lifetime of the $^4I_{11/2}$ state is shorter than that of the $^4I_{13/2}$ state, so the ESA process ($^4I_{13/2} \rightarrow {}^4F_{9/2}$) that populates the $^4F_{9/2}$ level responsible for red emission will be stronger.

By comparing radiative lifetimes of the excited states [$\tau_{rad} = \Sigma_{J'}A(JJ')$] and measured decay times for the luminescence from these states, τ_{exp}, we estimated the nonradiative decay-rate constants, $A_{NR} = (1/\tau_{exp}) - \Sigma_{J'}A(JJ')$, see Table 8. The value of A_{NR} is related to the energy gap ΔE between the considered state and the lower-lying state by the equation [42]:

$$A_{NR} = Ce^{-\alpha\Delta E}, \qquad (11)$$

where C and α are the constants characteristic of the host material. Eq. (11) is applicable for a constant temperature and concentration of active ions.

In Fig. 6(d), we plotted the obtained values of A_{NR} vs. the minimum energy gap ΔE_{min} between the excited-states calculated from the known structure of energy levels of Er^{3+} ions in the YSGG crystal. In a semi-log scale, this dependence was fitted by a linear law yielding $C = 3.4\times10^7$ s^{-1} and $\alpha = 2.0\times10^{-3}$ cm constants. The agreement between the calculated A_{NR} values and the best-fitting curve is satisfactory for the $^4I_{13/2}$, $^4I_{9/2}$, $^4F_{9/2}$ and $^4S_{3/2} + {}^2H_{11/2}$ states, while for the $^4I_{11/2}$ state the calculated A_{NR} value (666.6 s^{-1}) is one order of magnitude lower than one predicted from the linear fit (~8×10^4 s^{-1}). Thus, simple model described by Eq. (11) that is typically used for the description of nonradiative decay in Er^{3+}-doped materials with a relatively low Er^{3+} concentrations [43], predicts even stronger shortening of the luminescence lifetime of the $^4I_{11/2}$ state for Er:YSGG crystal. However, particularly long τ_{exp} value for this state makes Er:YSGG crystal attractive for laser operation on the $^4I_{11/2} \rightarrow {}^4I_{13/2}$ transition (i.e., as compared with Er:YAG).

The deviation of the experimental points on A_{NR} from the linear law is attributed to a very high concentration of Er^{3+} ions that could generate more complicated dependence between A_{NR} and ΔE. Indeed, the considered N_{Er} value (4.82×10^{21} at/cm^3) should be compared with the so-called quenching concentration N_q that corresponds to a reduction of the luminescence lifetime τ_{exp} with respect to the radiative one τ_{rad} by a factor of 2, $\tau_{exp} = \tau_{rad}/[1+(N_{Er}/N_q)^2]$ [44]. For Er^{3+} ions in YAG, N_q ~3×10^{21} at/cm^3 [45] (for the Er^{3+}:YSGG crystal, these data are not presented in the literature).

More significant shortening of τ_{exp} with respect to τ_{rad} for the $^4I_{11/2}$ state as compared with the $^4I_{13/2}$ state can be understood with Eq. (11) and the values of energy gaps ΔE_{min} for these states that are 3372 and 6370 cm^{-1}, respectively. If considering multi-phonon mechanism of the non-radiative decay, this means that ~5 and 9 phonons are required to depopulate theses states (here we consider the maximum vibrational frequency of YSGG, ν_{max} = 752 cm^{-1} [46]). Thus, for the $^4I_{11/2}$ state this process should have much higher probability. Another mechanism of shortening of the τ_{exp} value can be en-

ergy-transfer to the impurities ions that in enhanced with the increase of the Er^{3+} concentration [45]. The probability of this energy-transfer can be different for the $^4I_{11/2}$ and $^4I_{13/2}$ states depending on if they are resonant in energy to the impurity states; in addition, this process is strongly dependent on the growth method and particular composition of the considered sample [45].

4. Conclusions

We report on a comprehensive spectroscopic study of a highly-doped 38 at.% Er:YSGG crystal. Optical absorption and luminescence of Er^{3+} ions is studied. The maximum absorption cross-section for the $^4I_{15/2} \rightarrow {}^4I_{11/2}$ transition is $\sigma_{abs} = 0.46\times10^{-20}$ at 965.8 nm. Radiative lifetimes of all excited states of the Er^{3+} ion from $^4I_{13/2}$ to $^2H_{9/2}$, branching ratios and probabilities of radiative transitions from these states are determined using the Judd-Ofelt theory. Radiative lifetimes of the $^4I_{13/2}$ and $^4I_{11/2}$ excited states for Er^{3+} ions in YSGG crystal are 7.73 ms and 9.75 ms, respectively. Using these relevant spectroscopic data, stimulated-emission cross-section spectra are evaluated for ~1.5 μm ($^4I_{13/2} \rightarrow {}^4I_{15/2}$) and 3 μm ($^4I_{11/2} \rightarrow {}^4I_{13/2}$) transitions. For the $^4I_{11/2} \rightarrow {}^4I_{13/2}$ channel, the maximum stimulated-emission cross-section is 0.43×10^{-20} cm^2 at 2797.1 nm. The role of non-radiative relaxation on the shortening of luminescence lifetimes of lower excited-states of Er^{3+} is discussed.

References

1. H. Stange, K. Petermann, G. Huber, E. W. Duczynski, Appl. Phys. B 49 (1989) 269-273.
2. B. J. Dinerman, P. F. Moulton, Opt. Lett. 19 (1994) 1143-1145.
3. J.S. Liu, J.J. Liu, Y. Tang, Laser Phys. 18 (2008) 1124-1127.
4. A. Aubourg, J. Didierjean, N. Aubry, F. Balembois, P. Georges, Opt. Lett. 38 (2013) 938-940.
5. H. Jelinkova, T. Dostalova, K. Hamal, O. Krejsa, J. Kubelka, S. Prochazka, Laser Phys. 8 (1998) 176-181.
6. A. Zajac, M. Skorczakowski, J. Swiderski, P. Nyga, Opt. Express 12 (2004) 5125-5130.
7. M. Pollnau, W. Luthy, H.P. Weber, "*Influence of normal and inverse upconversion processes on the continuous wave operation of the Er^{3+} 3 μm crystal laser*", Vol. 20 of OSA Proceedings Series (Optical Society of America, 1994), P. EL5.
8. S. Georgescu, O. Toma, IEEE J. Selected Top. Quantum Electron. 11 (2005) 682-689.
9. V. Lupei, S. Georgescu, V. Florea, IEEE J. Quantum Electron. 29 (1993) 426-434.
10. S. Georgescu, O. Toma, H. Totia, IEEE J. Quantum Electron. 39 (2003) 722-732.
11. E. A. Arbabzadah, C. C. Phillips, M. J. Damzen, Appl. Phys. B 111 (2013) 333-339.
12. E. A. Arbabzadah, S. Chard, H. Amrania, C. C. Phillips, M. J. Damzen, Opt. Exp. 19 (2011) 25860-25865.
13. P. F. Moulton, J. G. Manni, and G. A. Rines, IEEE J. Quantum Electron. 24 (1998) 960-973.
14. E. Zharikov, N.N. Il'ichev, S.P. Kalitin, V.V. Laptev, A.A. Malyutin, V.V. Osiko, P.P. Pashinin, A.M. Prokhorov, Z.V. Saidov, V.A. Smirnov, A.F. Umyskov, I.A. Shcherbakov, Sov. J. Quantum Electron. 16 (1986) 635–639.
15. J.B. Gruber, J.R. Quagliano, M.F. Reid, F.S. Richardson, M.E. Hills, M.D. Seltzer, S.B. Stevens, C.A. Morrison, T.H. Allik, Phys. Rev. B 48 (1993) 15561-15573.
16. J. Su, C. Yang, Q. Li, Q. Zhang, J. Luo, J. Lumin. 130 (2010) 1546–1550.
17. D.K. Sardar, W.M. Bradley, J.J. Perez, J.B. Gruber, B. Zandi, J.A. Hutchinson, C.W. Trussell, M.R. Kokta, J. Appl. Phys. 93 (2003) 2602.
18. X.S. Chen, J. Collins, B. DiBartolo, B. Bowlby, B. Dinerman, D. Weyburne, J. Lumin. 72-74 (1997) 168.
19. X.S. Chen, T. Nguyen, Q. Luu, B. Dibartolo, J. Lumin. 83-84 (1999) 471.
20. Q.Y. Wang, S.Y. Zhang, Y.Q. Jia, J. Alloys & Cmpd. 202 (1993) 1.
R. Micheletti, P. Minguzzi, M. A. Noginov, M. Tonelli, J. Opt. Soc. Amer. B 11 (1994) 2095-2099.
21. B.R. Judd, Phys. Rev. 172 (1962) 750–761.
22. G.S. Ofelt, J. Chem. Phys. 37 (1962) 511–519.

23. E.V. Zharikov, V.F. Kitaeva, V.Y. Fedorovich, Sov. Phys. Solid State 31 (1989) 298–299.
24. A.A. Kaminski, A.G. Petrosyan, G.A. Denisenko, T.I. Butaeva, V.A. Fedorov, S.E. Sarkisov, Phys. Stat. Sol. (a) 71 (1982) 291.
25. I.A. Belova, F.A. Bolshchikov, Yu.K. Voronko, A.V. Malov, A.V. Popov, P.A. Ryabochkina, A.A. Sobol, S.N. Ushakov, Phys. Solid State 50 (2008) 1611.
26. W.F. Krupke, M.D. Shinn, J.E. Marion, J. Opt. Soc. Am. B 3 (1986) 102.
27. M.J. Weber, Phys. Rev. 171 (1968) 283.
28. A.A. Kaminski, V.S. Mironov, A.A. Kornienko, S.N. Bagaev, G. Boulon, A. Brenier, B. Di Bartolo, Phys. Stat. Sol. (a) 151 (1995) 231.
29. P.A. Tanner, C.S.K. Mak, M.D. Faucher, W.M. Kwok, D.L. Phillips, V. Mikhailik, Phys. Rev. B 67 (2003) 115102.
30. E.B. Dunina, A.A. Kornienko, L.A. Fomicheva, Cent. Eur. J. Phys. 6 (2008) 407–414.
31. M. Pollnau, D.R. Gamelin, S.R. Lüthi, H.U. Güdel, M.P. Hehlen, Phys. Rev. B 61 (2000) 3337 – 3346.
32. S.A. Payne, L.K. Smith, W.F. Krupke, J. Appl. Phys. 77 (1995) 4274.
33. M.J. Weber, Phys. Rev. 157 (1967) 262.
34. M. Pollnau, R. Spring, Ch. Ghisler, S. Wittwer, W. Luthy, H.P. Weber, IEEE J. Quantum Electron. 32 (1996) 657.
35. B.F. Aull, H.P. Jenssen, IEEE J. Quantum Electron. 18 (1982) 925–930.
36. A.S. Yasyukevich, V.G. Shcherbitskii, V.E. Kisel, A.V. Mandrik, N.V. Kuleshov, J. Appl. Spectr. 71 (2004) 202-208.
37. K. Spariosu, M. Birnbaum, M. Kokta, Appl. Opt. 34 (1995) 8272-8275.
38. M. Tikerpae, S.D. Jackson, T.A. King, J. Modern Opt. 45 (1998) 1269.
39. E.V. Zharikov, V.I. Zhekov, T.M. Murina, V.V. Osiko, M.L Timoshechkin, I.A. Shcherbakov, Sov. J. Quantum Electron. 7 (1977) 117.
40. D Koetke, G. Huber, Appl. Phys. B 61 (1995) 151.
41. T. Schweizer, T. Jensen, E. Heumann, G. Huber, Opt. Commun. 118 (1995) 557.
42. N. Yamada, S. Shionoya, T. Kushida, J. Phys. Soc. Jpn. 32 (1972) 1577–1586.
43. L. Agazzi, K. Wörhoff, A. Kahn, M. Fechner, G. Huber, M. Pollnau, J. Opt. Soc. Am. B 30 (2013) 663-677.
44. H. Higuchi, M. Takahashi, Y. Kawamoto, K. Kadono, T. Ohtsuki, N. Peyghambarian, N. Kitamura, J. Appl. Phys. 83 (1998) 19-27.
45. S. Georgescu, V. Lupei, A. Lupei, V. I. Zhekov, T. M. Murina, M. I. Studenikin, Opt. Commun. 81 (1991) 186-192.
46. D. Chiriu, P.C. Ricci, C.M. Carbonaro, A. Anedda, M. Aburish-Hmidat, A. Grosu, P.G. Lorrai, E. Fortin, J. Appl. Phys. 100 (2006) 033101.

List of figure captions

Figure 1 Erbium energy level diagram.

Figure 2 Absorption cross-section spectra for 38 at.% Er:YSGG crystal.

Figure 3 (a) Near-IR luminescence from 38 at.% Er:YSGG crystal, bands at 0.95–1.7 μm and 2.6–3 μm are not in scale; (b) up-conversion luminescence (UCL) from this crystal, excitation wavelength is 962 nm.

Figure 4 Dependence of the UCL intensity on the excitation power density for 38 at.% Er:YSGG, *points* are the experimental data, *lines* are their fitting for the slope (*n*) calculation.

Figure 5 Stimulated-emission cross-section σ_{SE} spectra for the $^4I_{13/2} \rightarrow {}^4I_{15/2}$ (a) and $^4I_{11/2} \rightarrow {}^4I_{13/2}$ (c) transitions of Er^{3+} ions in Er:YSGG crystal, as calculated with the reciprocity, Eq. (7) and Füchtbauer–Ladenburg (F–L) methods, Eq. (6); gain cross-section, $\sigma_g = \beta\sigma_{SE}-(1-\beta)\sigma_{abs}$, spectrum for the $^4I_{13/2} \rightarrow {}^4I_{15/2}$ transition (b), β is the inversion ratio.

Figure 6 Luminescence decay curves for emissions from the $^4I_{13/2}$, $^4I_{11/2}$ (a), $^4I_{9/2}$ (b), $^4F_{9/2}$ and $^4S_{3/2}$ (c) excited-states of Er^{3+} ions in the 38 at.% Er:YSGG crystal under resonant excitation; (d) energy-gap dependence of the nonradiative decay-rate constants A_{NR} in 38 at.% Er:YSGG in a semi-log scale: *points* are the values determined with the measured luminescence lifetimes and the calculated radiative decay rate constants, *line* is the fit through these data with Eq. (11).

Table 1 Absorption oscillator strengths f_{exp} [determined from the absorption spectra, Eq. (1)], f_{calc} (calculated by means of J-O theory) and integrated absorption coefficient Γ for Er^{3+} ion in the YSGG crystal.

Transition $^4I_{15/2} \rightarrow$	Wavenumbers, cm^{-1}	Γ, $nm \cdot cm^{-1}$	Absorption oscillator strengths*, 10^{-6}	
			f_{exp}	f_{calc}
$^4I_{13/2}$	6278 – 6592	697.6	0.676	$0.647^{ed}+0.564^{md}$
$^4I_{11/2}$	10188 – 10389	177.1	0.439	0.254
$^4I_{9/2}$	12310 – 12731	79.5	0.290	0.378
$^4F_{9/2}$	15223 – 15460	287.9	1.588	1.768
$^4S_{3/2}$	18371 – 18474	44.3	0.352	0.213
$^2H_{11/2}$	19035 – 19436	342.9	2.972	3.348
$^4F_{7/2}$	20457 – 20640	123.9	1.226	1.188
$^4F_{5/2}$	22254 – 22508	36.3	0.419	0.258
$^4F_{3/2}$	22583 – 22646	26.4	0.317	0.151
$(^2G,^4F,^2H)_{9/2}$	24367 – 24773	42.1	0.595	0.371
$^4G_{11/2}$	26151 – 26643	375.3	6.127	5.921
$^4G_{7/2+}{}^4G_{9/2}+{}^2K_{15/2}$	27254 – 28148	114.8	2.063	$1.784^{ed}+0.067^{md}$
$(^2P,^2D,^4F)_{3/2}$	31439 – 31579	3.6	0.084	0.029
$^2K_{13/2}$	33093 – 33676	11.6	0.303	0.060
$^4G_{5/2}+{}^2P_{1/2}$	–			
$^4G_{7/2}$	33950 – 34150	6.2	0.168	0.201
$^2D_{5/2}$	34728 – 34894	3.1	0.088	0.042
$(^2H,^2G)_{9/2}$	36279 – 36514	17.9	0.556	0.312
rms dev.				*0.245*

* Superscripts ED and MD represent contribution of electric-dipole and magnetic-dipole transitions, respectively. Numbers without superscripts correspond to pure ED transitions.

Table 2 Judd-Ofelt parameters Ω_k (k = 2, 4, 6) and spectroscopic quality factors $X_{2/6} = \Omega_2/\Omega_6$ and $X_{4/6} = \Omega_4/\Omega_6$ for various Er^{3+}-doped crystals.

Crystal	Judd-Ofelt parameters, Ω_k (k = 2, 4, 6), 10^{-20} cm^2			Spectroscopic quality factors		Ref.
	Ω_2	Ω_4	Ω_6	$X_{2/6}$	$X_{4/6}$	
Er:YSGG	2.22	1.50	0.46	*4.82*	*3.26*	This work
	0.23	0.86	0.37	*0.62*	*1.62*	[16]
	0.92	0.48	0.87	*1.06*	*0.55*	[17]
Er:GGG	0.70	0.37	0.86	*0.81*	*0.43*	[17]
Er:YAG	0.47	0.96	0.61	*0.52–8.9**	*1.57–2.11**	[24]
Er:LuAG	0.47	1.04	0.7	*0.60–11.4**	*1.47–2.11**	[24]
Er:CNGG	3.74	3.15	2.58	*1.45*	*1.22*	[25]
Er:GSGG	0.35	2.35	3.23	*0.11*	*0.73*	[26]
Er:Y_2O_3	4.59	1.21	0.48	*9.56*	*2.52*	[27]
Er:$YAlO_3$	0.95	0.58	0.55	*1.72*	*1.05*	[28]

*Taking into account hyper-sensitive Er^{3+} transitions

Table 3 Luminescence branching ratios *B*(JJ') for Er^{3+} ions in YSGG calculated with the Judd-Ofelt theory.

Initial state	Final state	*B*(JJ')
$^4I_{13/2}$	$^4I_{15/2}$	1.0
$^4I_{11/2}$	$^4I_{15/2}$	0.746
	$^4I_{13/2}$	0.254
$^4I_{9/2}$	$^4I_{15/2}$	0.868
	$^4I_{13/2}$	0.120
	$^4I_{11/2}$	0.012
$^4F_{9/2}$	$^4I_{15/2}$	0.923
	$^4I_{13/2}$	0.046
	$^4I_{11/2}$	0.028
	$^4I_{9/2}$	0.003
$^4S_{3/2}$	$^4I_{15/2}$	0.660
	$^4I_{13/2}$	0.270
	$^4I_{11/2}$	0.022
	$^4I_{9/2}$	0.048
	$^4F_{9/2}$	<0.001
$^2H_{11/2}$	$^4I_{15/2}$	0.917
	$^4I_{13/2}$	0.050
	$^4I_{11/2}$	0.019
	$^4I_{9/2}$	0.012
	$^4F_{9/2}$	0.003
	$^4S_{3/2}$	<0.001
$^4F_{7/2}$	$^4I_{15/2}$	0.674
	$^4I_{13/2}$	0.208
	$^4I_{11/2}$	0.077
	$^4I_{9/2}$	0.033
	$^4F_{9/2}$	0.007
	$^4S_{3/2}$	<0.001
	$^2H_{11/2}$	<0.001
$^4F_{5/2}$	$^4I_{15/2}$	0.345
	$^4I_{13/2}$	0.488
	$^4I_{11/2}$	0.075
	$^4I_{9/2}$	0.039
	$^4F_{9/2}$	0.051
	$^4S_{3/2}$	<0.001
	$^2H_{11/2}$	0.001
	$^4F_{7/2}$	<0.001
$^4F_{3/2}$	$^4I_{15/2}$	0.371
	$^4I_{13/2}$	0.036
	$^4I_{11/2}$	0.372
	$^4I_{9/2}$	0.207
	$^4F_{9/2}$	0.007
	$^4S_{3/2}$	0.007
	$^2H_{11/2}$	<0.001
	$^4F_{7/2}$	<0.001
	$^4F_{5/2}$	<0.001
$(^2G,^4F,^2H)_{9/2}$	$^4I_{15/2}$	0.346
	$^4I_{13/2}$	0.448
	$^4I_{11/2}$	0.141
	$^4I_{9/2}$	0.010
	$^4F_{9/2}$	0.040
	$^4S_{3/2}$	<0.001
	$^2H_{11/2}$	0.010
	$^4F_{7/2}$	0.003
	$^4F_{5/2}$	<0.001
	$^4F_{3/2}$	<0.001

Table 4 Luminescence branching ratios $B(JJ')$ from the $^4I_{11/2}$ excited-state for Er^{3+} ions in various crystals.

Crystal	$B(^4I_{11/2} \rightarrow {}^4I_{15/2})$	$B(^4I_{11/2} \rightarrow {}^4I_{13/2})$	Ref.
Er:YSGG	74.6%	25.4%	This work
	72.6%	27.4%	[16]
	88.7%	11.3%	[17]
Er:GGG	88.8%	11.2%	[17]
	78%	22%	[32]
Er:GSGG	77%	23%	[32]
Er:YAG	80.2%	19.8%	[24]
Er:LuAG	81.2%	18.8%	[24]
Er:Y_2O_3	81.3%	18.7%	[27]
Er:KY_3F_{10}	73%	27%	[32]

Table 5 Lifetimes of the excited-states for Er:YSGG crystal*.

Excited state	Er:YSGG / calculated			Er:YSGG / measured	
	This work	Ref. [16]	Ref. [17]	This work	Ref. [2]
	τ_{rad}, μs	τ_{rad}, μs	τ_{rad}, μs	τ_{exp}, μs	τ_{exp}, μs
$^4I_{13/2}$	7731	6615	7919	2235	3400
$^4I_{11/2}$	9747	8868	5652	1300	1300
$^4I_{9/2}$	4270	5706	6998	0.35	–
$^4F_{9/2}$	653	812	778	10.2	–
$^4S_{3/2}$	1078	874	437	0.4	–
$^2H_{11/2}$	261	538	326	0.4	–
$^4F_{7/2}$	316	336	250	–	–
$^4F_{5/2}$	484	464	378	–	–
$^4F_{3/2}$	562	521	–	–	–
$(^2G,^4F,^2H)_{9/2}$	448	1711	–	–	–
$^4G_{11/2}$	71	–	–	–	–

*τ_{rad} – radiative lifetimes calculated with the Judd-Ofelt theory;
τ_{exp} – lifetime determined from the PL decay

Table 6 Radiative lifetimes τ_{rad} of the $^4I_{13/2}$ and $^4I_{11/2}$ excited-states for Er^{3+} ions in various crystals.

Crystal	$\tau_{rad}(^4I_{13/2})$, ms	$\tau_{rad}(^4I_{11/2})$, ms	Ref.
Er:YSGG	7.73	9.75	This work
Er:GGG	7.64	5.48	[17]
Er:YAG	7.3	8.8	[24]
Er:LuAG	6.8	7.8	[24]
Er:Y_2O_3	7.75	6.81	[27]
Er:LaF_3	10.9	11.6	[33]
Er:YLF	10.0	6.7	[34]

Table 7 Stimulated-emission cross-sections σ_{SE} for the $^4I_{11/2} \rightarrow {}^4I_{13/2}$ and $^4I_{13/2} \rightarrow {}^4I_{15/2}$ transitions of Er^{3+} ions in various crystals.

Crystal	σ_{SE}, 10^{-20} cm^2		Ref.
	$^4I_{11/2} \rightarrow {}^4I_{13/2}$	$^4I_{13/2} \rightarrow {}^4I_{15/2}$	
Er:YSGG	0.43	1.20	This paper
	2.8	–	[38]
Er:YAG	0.56	0.72	[39,40]
Er:GSGG	2.9	–	[32]
Er:$YAlO_3$	–	0.55	[40]
Er:YSO	–	1.0	[41]
Er:YLF	1.2	–	[38]
Er:KY_3F_{10}	1.9	–	[32]

Table 8 Energy gaps to the next lower levels, total radiative decay-rate constants, radiative and luminescence lifetimes, and nonradiative decay-rate constants of the lowest five excited states* of Er^{3+} in YSGG.

State	E, cm^{-1} [15]	ΔE_{min}, cm^{-1}	$\Sigma_{J'}A(JJ')$, s^{-1}	τ_{rad}, ms	τ_{exp}, ms	A_{NR},** s^{-1}
$^4I_{15/2}$	0 – 502	–	–	–	–	–
$^4I_{13/2}$	6553 – 6872	6370	129.3	7.73	2.24	318.1
$^4I_{11/2}$	10244 – 10403	3372	102.6	9.75	1.30	666.6
$^4I_{9/2}$	12296 – 12734	1893	234.2	4.27	0.4	2.85×10^6
$^4F_{9/2}$	15310 – 15527	2576	1531	0.65	10.2	9.65×10^4
$^4S_{3/2}+^2H_{11/2}$	18407 – 19367	2880	4757	0.21	0.4	2.50×10^6

*The $^4S_{3/2}$ and $^2H_{11/2}$ levels are treated as a single, thermally coupled level.

** $A_{NR} = (1/\tau_{exp}) - \Sigma_{J'}A(JJ')$.

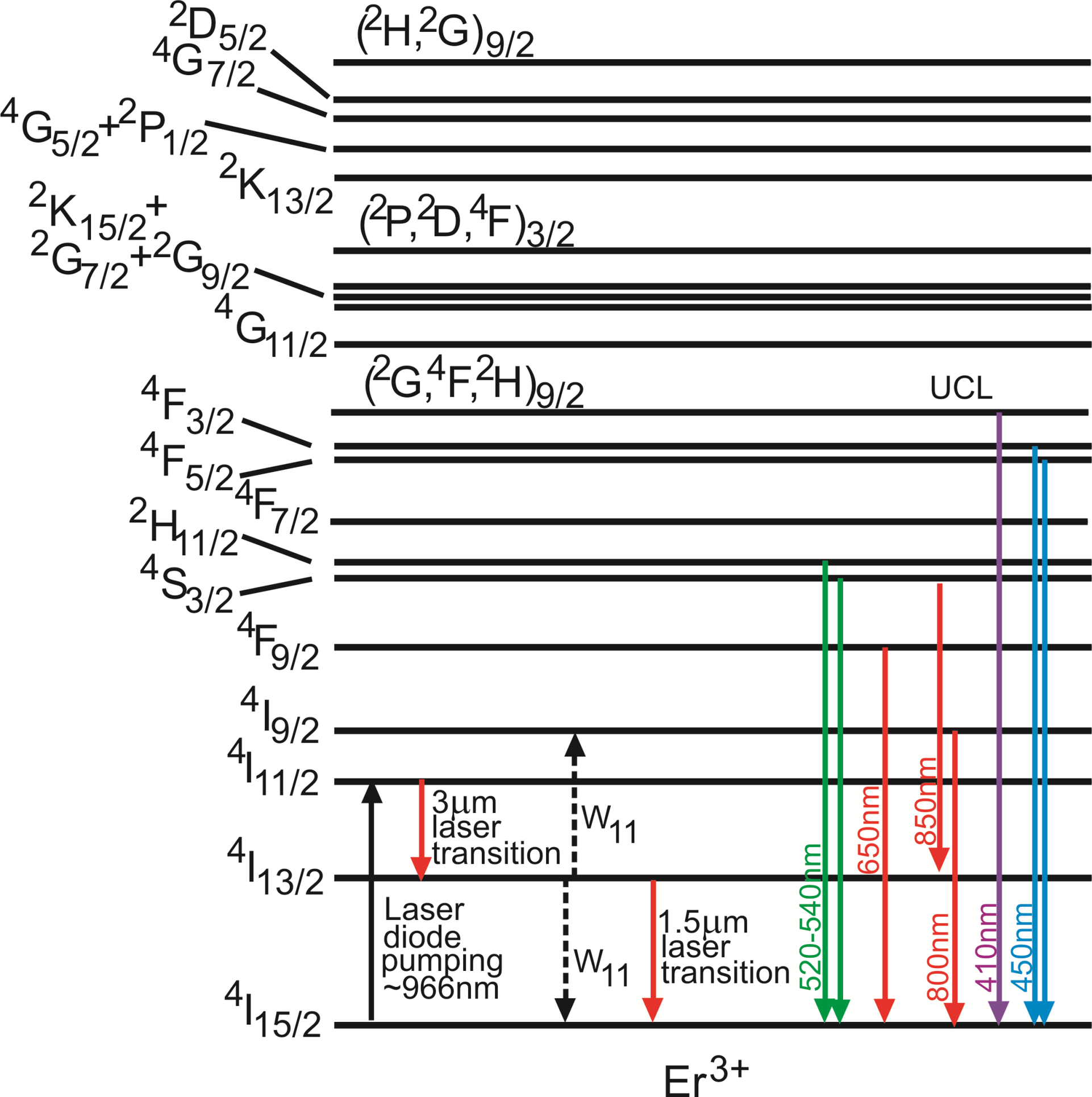
$^2D_{5/2}$
$^4G_{7/2}$
$(^2H,^2G)_{9/2}$
$^4G_{5/2}+^2P_{1/2}$
$^2K_{13/2}$
$^2K_{15/2}+$
$^2G_{7/2}+^2G_{9/2}$
$(^2P,^2D,^4F)_{3/2}$
$^4G_{11/2}$
$(^2G,^4F,^2H)_{9/2}$
UCL
$^4F_{3/2}$
$^4F_{5/2}$
$^4F_{7/2}$
$^2H_{11/2}$
$^4S_{3/2}$
$^4F_{9/2}$
$^4I_{9/2}$
$^4I_{11/2}$
$^4I_{13/2}$
$^4I_{15/2}$
3µm laser transition
W_{11}
Laser diode pumping ~966nm
W_{11}
1.5µm laser transition
520-540nm
650nm
850nm
800nm
410nm
450nm
Er^{3+}

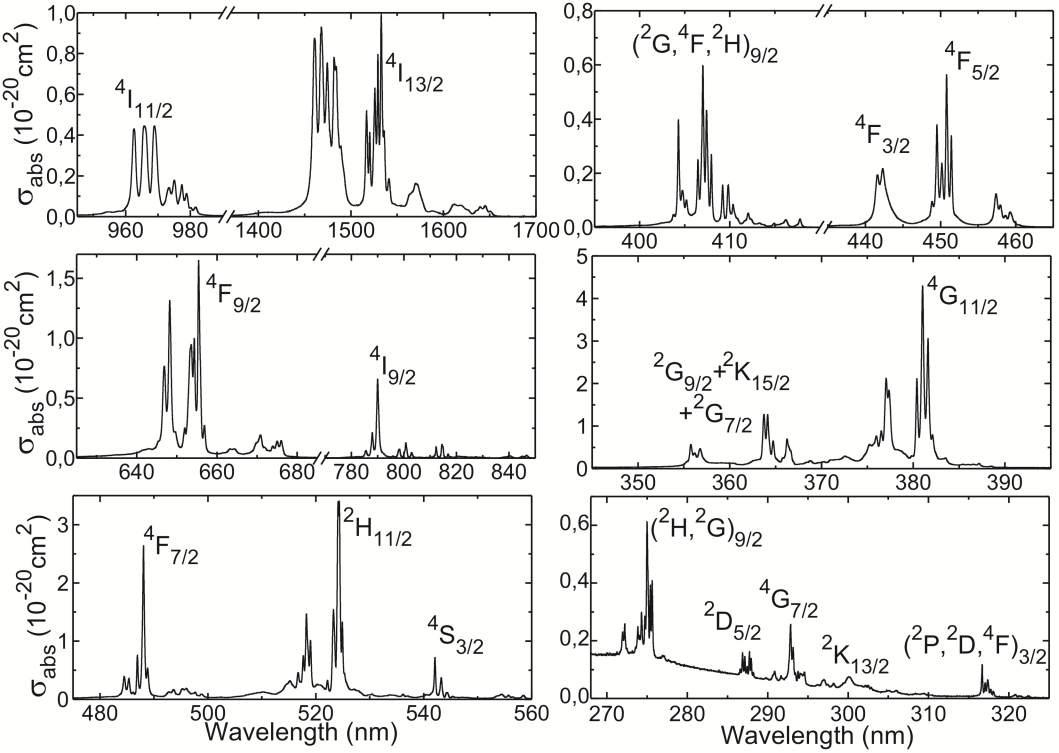
σabs (10-20cm2)
4I11/2
4I13/2
(2G,4F,2H)9/2
4F5/2
4F3/2
4F9/2
4I9/2
4G11/2
2G9/2+2K15/2
+2G7/2
4F7/2
2H11/2
4S3/2
(2H,2G)9/2
2D5/2
4G7/2
2K13/2
(2P,2D,4F)3/2
Wavelength (nm)

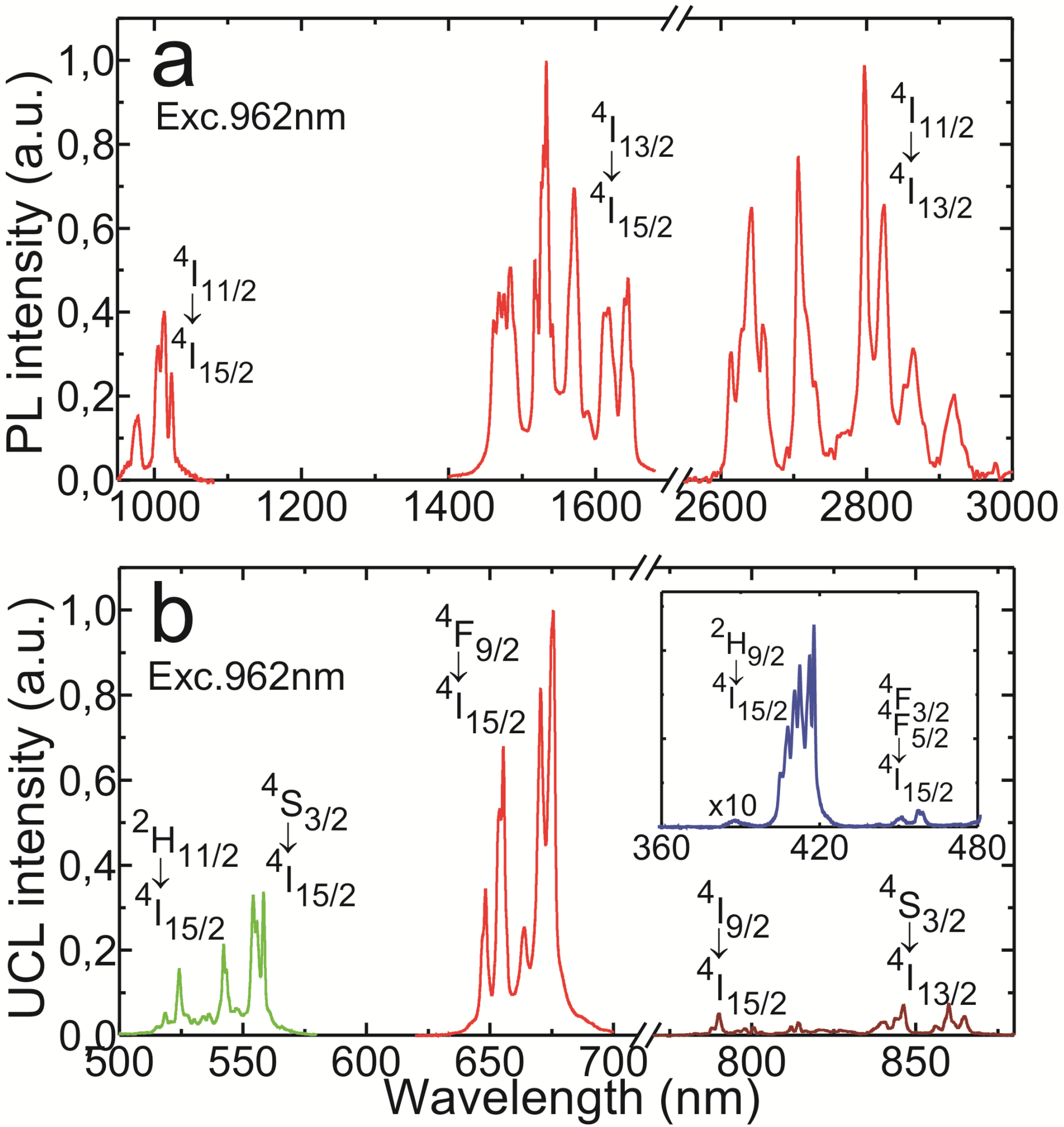
a
Exc.962nm
PL intensity (a.u.)
1,0
0,8
0,6
0,4
0,2
0,0
1000
1200
1400
1600
2600
2800
3000
$^4I_{11/2}$ → $^4I_{15/2}$
$^4I_{13/2}$ → $^4I_{15/2}$
$^4I_{11/2}$ → $^4I_{13/2}$
b
Exc.962nm
UCL intensity (a.u.)
1,0
0,8
0,6
0,4
0,2
0,0
500
550
600
650
700
800
850
Wavelength (nm)
$^2H_{11/2}$ → $^4I_{15/2}$
$^4S_{3/2}$ → $^4I_{15/2}$
$^4F_{9/2}$ → $^4I_{15/2}$
$^4I_{9/2}$ → $^4I_{15/2}$
$^4S_{3/2}$ → $^4I_{13/2}$
$^2H_{9/2}$ → $^4I_{15/2}$
$^4F_{3/2}$, $^4F_{5/2}$ → $^4I_{15/2}$
x10
360
420
480

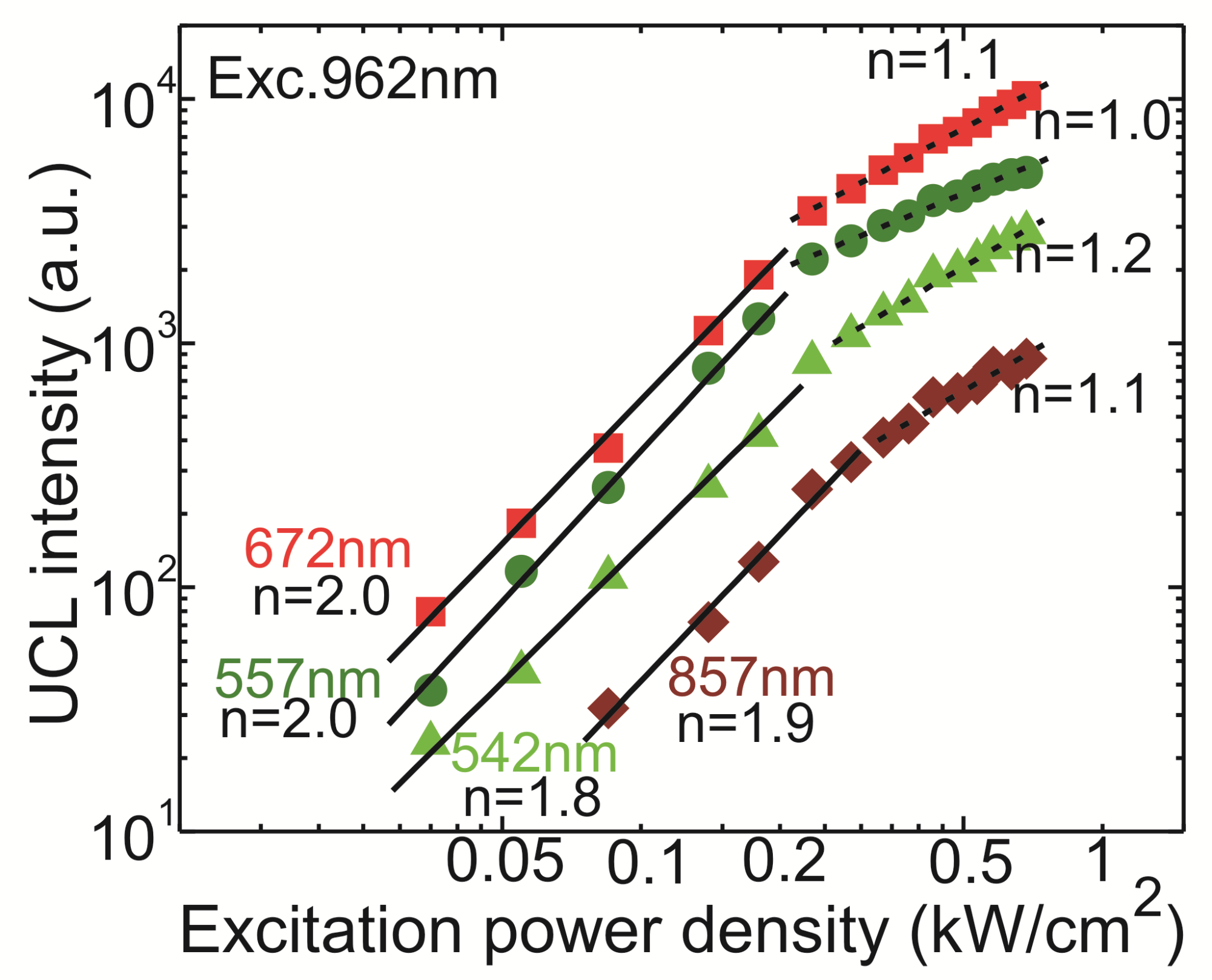
Exc.962nm
n=1.1
n=1.0
n=1.2
n=1.1
672nm
n=2.0
557nm
n=2.0
542nm
n=1.8
857nm
n=1.9
UCL intensity (a.u.)
10^4
10^3
10^2
10^1
0.05
0.1
0.2
0.5
1
Excitation power density (kW/cm^2)

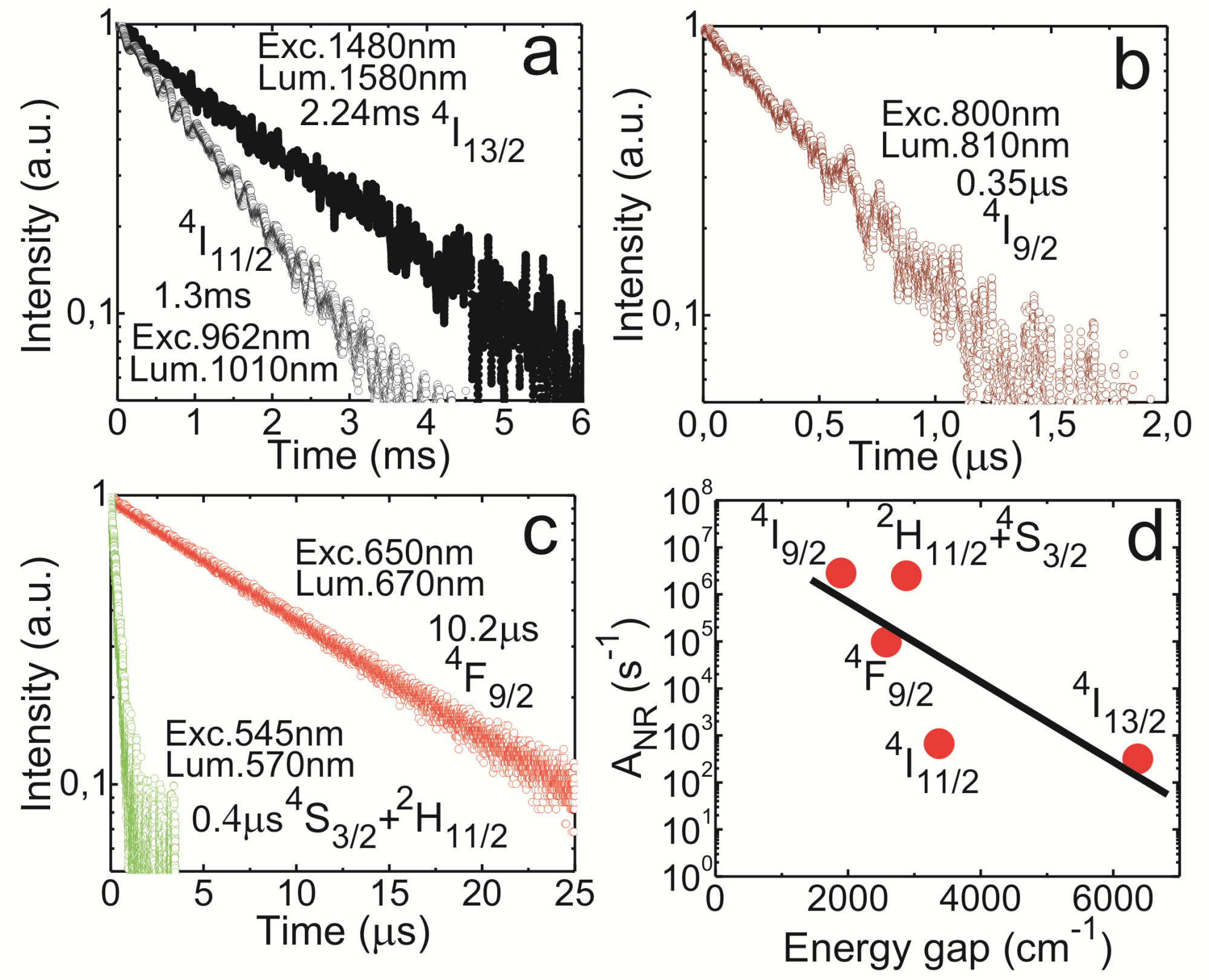
a
Exc.1480nm
Lum.1580nm
2.24ms $^4I_{13/2}$
$^4I_{11/2}$
1.3ms
Exc.962nm
Lum.1010nm
Intensity (a.u.)
Time (ms)
b
Exc.800nm
Lum.810nm
0.35μs
$^4I_{9/2}$
Intensity (a.u.)
Time (μs)
c
Exc.650nm
Lum.670nm
10.2μs
$^4F_{9/2}$
Exc.545nm
Lum.570nm
0.4μs $^4S_{3/2}$+$^2H_{11/2}$
Intensity (a.u.)
Time (μs)
d
$^4I_{9/2}$
$^2H_{11/2}$+$^4S_{3/2}$
$^4F_{9/2}$
$^4I_{13/2}$
$^4I_{11/2}$
A_{NR} (s^{-1})
Energy gap (cm^{-1})

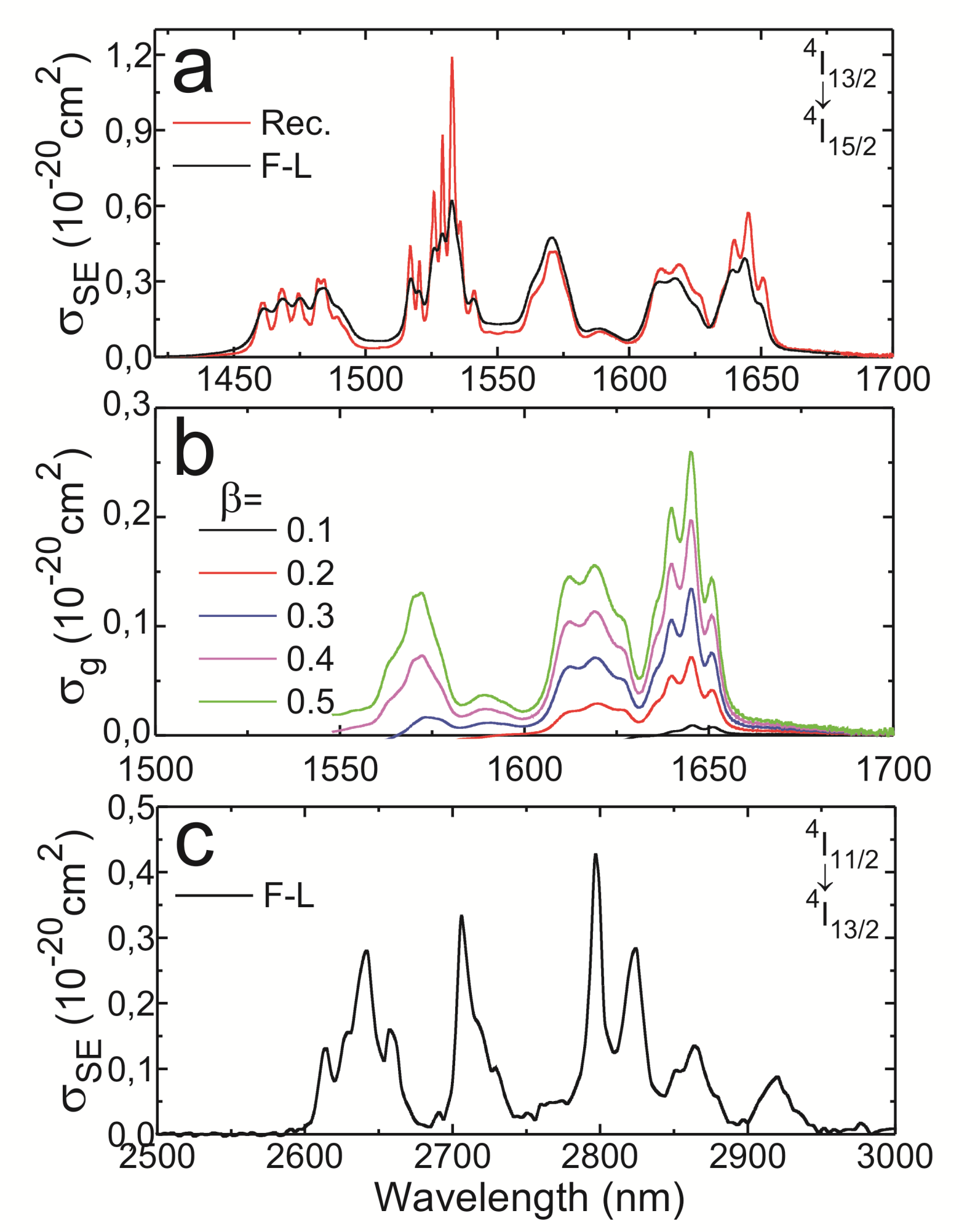
a
Rec.
F-L
$^4I_{13/2}$
$^4I_{15/2}$
σ_{SE} (10^{-20}cm^2)
1,2
0,9
0,6
0,3
0,0
1450
1500
1550
1600
1650
1700
b
β=
0.1
0.2
0.3
0.4
0.5
σ_g (10^{-20}cm^2)
0,3
0,2
0,1
0,0
1500
1550
1600
1650
1700
c
F-L
$^4I_{11/2}$
$^4I_{13/2}$
σ_{SE} (10^{-20}cm^2)
0,5
0,4
0,3
0,2
0,1
0,0
2500
2600
2700
2800
2900
3000
Wavelength (nm)

Judd-Ofelt analysis and stimulated-emission cross-sections for highly doped (38 at.%) Er:YSGG laser crystal

P.A. Loiko[1,*], E. A. Arbabzadah[2], M. J. Damzen[2],
X. Mateos[3], E.B. Dunina[4], A.A. Kornienko[4],
A.S. Yasukevich[1], N.A. Skoptsov[1] and K.V. Yumashev[1]

[1] *Center for Optical Materials and Technologies, Belarusian National Technical University, 65/17 Nezavisimosti Ave., Minsk 220013, Belarus*
[2] *Photonics, The Blackett Laboratory, Imperial College London, London SW7 2BW, UK*
[3] *Física i Cristal·lografia de Materials i Nanomaterials (FiCMA-FiCNA), Universitat Rovira i Virgili (URV), Campus Sescelades, c/ Marcel·lí Domingo, s/n., Tarragona, Spain E-43007*
[4] *Vitebsk State Technological University, 72 Moskovskaya Ave., Vitebsk, Belarus 210035*

**Corresponding author e-mail: kinetic@tut.by*
Tel. +375(17)2939188, Fax. +375(17)2926286

Abstract Stimulated-emission cross-section spectra are determined for the ~1.5 μm and 3 μm transitions of Er^{3+} ions in YSGG crystal. For the $^4I_{11/2} \rightarrow {}^4I_{13/2}$ channel, the maximum stimulated-emission cross-section σ_{SE} is 0.43×10^{-20} cm^2 at 2797.1 nm. For the $^4I_{13/2} \rightarrow {}^4I_{15/2}$ channel, $\sigma_{SE} = 1.20\times10^{-20}$ cm^2 at 1532.8 nm. Due to the reabsorption loss, laser operation is expected at ~1644 nm. Radiative lifetimes of all excited states of the Er^{3+} ion from $^4I_{13/2}$ to $^2H_{9/2}$ and probabilities of radiative transitions from these states are determined using the Judd-Ofelt theory. Radiative lifetimes of the $^4I_{13/2}$ and $^4I_{11/2}$ excited states for Er^{3+} ions in YSGG are 7.73 ms and 9.75 ms, respectively. Non-radiative decay is analyzed for lower excited-states of Er^{3+} ions in YSGG.

Keywords: erbium ions; gallium garnets; Judd-Ofelt analysis; stumulated emission

1. Introduction

Erbium-doped garnets are widely used as laser crystals for the generation of ~1.5 and 3 μm radiation [1-4]. The 3 μm transition of Erbium doped lasers falls at a peak in the water absorption spectrum making laser sources at this wavelength extremely useful in medicine and dentistry [5,6]. A difficulty associated with this laser transition is that the lower laser level ($^4I_{13/2}$) has a longer lifetime than the upper laser level ($^4I_{11/2}$), which would usually result in self terminating behavior [7-10]. However, with highly doped Erbium crystals this effect can be counteracted via energy transfer upconversion (ETU) processes which recycle population from the lower laser level back to the upper laser level (and are stronger at higher doping levels when the Er^{3+}–Er^{3+} inter-ionic distance is less) [7-10]. This mechanism is shown in Fig. 1 (labeled W_{11}) which is an energy level diagram for the system.

For successful laser construction and theoretical modeling of ~3 μm laser systems it is necessary to have accurate spectroscopic data on highly doped Erbium crystals. The majority of 3 μm laser studies on Erbium doped garnets has been undertaken using Er:YAG, but an interesting competitor for this material is Er:$Y_3Sc_2Ga_3O_{12}$ (Er:YSGG) [11,12]. This crystal has a significantly longer upper laser level lifetime for the ~3 μm transition, $^4I_{11/2}$, compared to Er:YAG (1.3 ms vs. 120 μs [2]), providing better energy storage potential which could translate into superior Q-switched performance. Moreover the shorter lower laser level lifetime of Er:YSGG compared to Er:YAG [2] could prove advantageous in reducing the likelihood of self-termination of the 3 μm transition. Spectroscopic properties of Er,Cr:YSGG were studied in [13,14]. Previous papers on Er:YSGG focused on structure of energy-levels of Er^{3+} ions [15], Judd-Ofelt modeling [16,17] and up- conversion luminescence [18,19]. However, some relevant spectroscopic parameters of the Er:YSGG material are still not well known, specifically the stimulated emission cross section for both the ~1.5 and 3 μm transition.

In this work, a detailed spectroscopic study of a highly doped 38 at.% Er:YSGG crystal is undertaken. Absorption and luminescence spectra are presented and stimulated emission cross sections are calculated for the ~1.5 and 3 μm laser transitions. The radiative lifetimes of the relevant excited states of the Erbium system are calculated using the conventional Judd-Ofelt (J–O) theory. Furthermore, the luminescence branching ratios, absorption oscillator strengths and probabilities of spontaneous radiative transitions are determined.

2. Experimental

The studied crystal was $Y_3Sc_2Ga_3O_{12}$ (YSGG) doped with 38 at.% Er. The Er concentration, N_{Er}, determined with Electron Probe MicroAnalysis (EPMA) was 48.2×10^{20} at/cm^3. Such a high Er content was selected as it corresponded to the typical doping levels (30...50 at.%) for Er:YSGG active elements used in ~3 μm lasers reported so far [2,11,12]. In addition, we aimed to study the influence of high doping level on the spectroscopic parameters of Er^{3+} ions. Indeed, as the ionic radius of six-fold oxygen-coordinated Y^{3+} ion (0.90 Å) is slightly larger than that of Er^{3+} ion (0.89 Å), high-level crystal doping can induce slight variation of the crystal structure and, hence, f-f transition intensities. For instance, this effect was observed for 0.5–29 at.% Er-doped YAG crystals [20].

Optical absorption spectra of Er:YSGG were measured with a Varian CARY 5000 spectrophotometer at room-temperature (RT, ~293 K). The spectral bandwidth (SBW) was ~0.02 nm. To avoid saturation of the detector, the sample used for absorption measurements was a thin (thickness: 100 μm) polished plate.

Photoluminescence (PL) of Er^{3+} ions was excited by the focused output of a 962 nm InGaAs laser diode (the maximum power density on the sample was ~1 kW/cm^2). The PL was collected in the direction perpendicular to the excitation direction by a wide-aperture lens. The spectrum was registered by means of a lock-in amplifier, monochromator MDR-23 (SBW ~0.2 nm) and sensitive Hamamatsu C5460-01 (0.4–0.9 μm) and G5851 (0.9–1.7 μm) photodetectors. The monochomator was calibrated with Xe lamp. The emission of the Er^{3+} ions at ~3 μm was detected with a compact

Fourier transform infrared spectrometer, FT-IR Rocket from Arcoptix. As an excitation source, Ti:Sapphire laser tuned to ~962 nm was used.

For the luminescence decay measurements, an optical parametric oscillator Lotis TII LT-2214 tuned to 545, 650, 800, 960 or 1480 nm was used as the excitation source; the duration of the excitation pulse was ~20 ns. The PL was collected by a wide-aperture lens and re-imaged to the input slit of the monochromator MDR-12 (SBW ~1 nm), before detection by a fast Hamamatsu C5460 or G5851 photodetector (response time, 40 ns) and 500 MHz Textronix TDS-3052B digital oscilloscope.

3. Results and discussion

The absorption spectrum of the Er:YSGG crystal is shown in Fig. 2. The absorption band related to the $^4I_{15/2} \rightarrow {}^4I_{11/2}$ transition, used for pumping of Er:YSGG crystals with InGaAs laser diodes, contains three intense peaks centered at 962.5, 965.8 and 968.8 nm. The corresponding absorption cross-section, σ_{abs}, is ~0.46×10^{-20} cm^2. Full width at half maximum (FWHM) for these peaks is relatively small, <1.5 nm. For the band related to the $^4I_{15/2} \rightarrow {}^4I_{13/2}$ transition, typically used for the resonant (inband) pumping of Er^{3+} lasers, the maximum σ_{abs} value is 1.02×10^{-20} cm^2 at 1532.6 nm. The spectral features determined for 38 at.% Er:YSGG crystal are similar to one reported in [16,17] for the same crystal with a lower Er doping level.

Absorption oscillator strengths for Er^{3+} ions were calculated directly from the measured absorption spectrum $\alpha(\lambda)$:

$$f_{\exp} = \frac{m_e c^2}{\pi e^2 N_{Er} \bar{\lambda}^2} \int \alpha(\lambda) d\lambda , \quad (1)$$

where $\bar{\lambda}$ is the coordinate of a "center of gravity" of the selected absorption band (mean wavelength), N_{Er} is the concentration of Er^{3+} ions, m_e and e are the electron mass and charge, respectively; the integration is performed over the absorption band.

In addition, absorption oscillator strengths were calculated from the line strength S(JJ') modeled within the conventional Judd-Ofelt (J–O) theory [21,22]:

$$S_{ED}(JJ') = \sum_k e^2 \Omega_k \, |\langle \gamma J \| U^k \| \gamma' J' \rangle|^2 . \quad (2)$$

Here, the summation is performed for k = 2, 4, 6; $|\langle \gamma J \| U^k \| \gamma' J' \rangle|^2$ is the square of reduced matrix element of the unit matrix U^k, E_J and $E_{J'}$ are the energies of γJ and $\gamma' J'$ multiplets, $\{\Omega_2, \Omega_4$ and $\Omega_6\}$ are the intensity (J–O) parameters. An expression for the calculation of f values from the corresponding line strengths is:

$$f_{ED} = \frac{8\pi^2 m_e c}{3(2J+1)\bar{\lambda} h e^2} \frac{(n^2+2)^2}{9n} S_{ED}(JJ') , \quad (3)$$

where n is the crystal refractive index [23] at the wavelength of $\bar{\lambda}$. J-O theory allows for a calculation of the line strengths for electric-dipole (ED) transitions. The contribution of magnetic-dipole (MD) transitions with J–J' =0,±1 was calculated separately using the Russell- Saunders approximation on wave functions of Er^{3+} ions under the assumption of a free-ion. Total calculated oscillator strengths were then $f_{calc} = f_{ED} + f_{MD}$. Prior to the fitting of experimental oscillator strengths with the J-O model, MD contributions were subtracted from the f_{exp} values.

The wave functions in the intermediate coupling scheme (ICS) corresponding to the states (energy levels) of the rare-earth ions are linear combinations of wave functions in the Russell-Saunders approximation (the L-S coupling scheme). The energy levels are designated usually by means of one or more L-S wave functions which contribute mainly to this linear combination. For designating of high-lying excited-states of Er^{3+} (see Fig. 1), we used this system. This means that the L-S wave functions $(^2G,{}^4F,{}^2H)_{9/2}$, $(^2P,{}^2D,{}^4F)_{3/2}$ and $(^2H,{}^2G)_{9/2}$ contribute mainly to the ICS wave function of Er^{3+} with energy level of ~24550 cm^{-1}, 31600 cm^{-1} and 36550 cm^{-1}, respectively.

Results on the experimental and calculated absorption oscillator strengths of Er^{3+} ions are presented in Table 1. For J–O theory, the obtained parameters are Ω_2 =2.22, Ω_4 =1.50 and Ω_6 =0.46 [10^-

^{20} cm^2]. In Table 2, we compared obtained J–O parameters with the ones reported previously for Er:YSGG [16,17] and different Er-doped crystals [24-28]. In addition, spectroscopy quality factors, $X_{2/6} = \Omega_2/\Omega_6$ and $X_{4/6} = \Omega_4/\Omega_6$, introduced by Kaminski [24], are calculated. They are used to estimate the potential of active materials for laser operation as they are linked to the luminescence branching ratios. For Er:YSGG, $X_{2/6} = 4.82$ and $X_{4/6} = 3.26$ that agrees with the range determined by Kaminski [24], Table 2. J–O parameters obtained in the present paper for 38 at.% Er:YSGG are different from the ones reported by Su et al. for 30 at.% Er:YSGG [16], Ω_2 =0.23, Ω_4 =0.86 and Ω_6 =0.37 and by Sardar et al. for 1 at.% Er:YSGG [17], Ω_2 =0.92, Ω_4 =0.48 and Ω_6 =0.87 [10^{-20} cm^2]. This is partially referred to the difference in Er concentration. Indeed, J–O parameters are sensitive to the intensities of hypersensitive Er^{3+} transitions [24] which are in turn affected by the crystal field.

It is well known that the excited configurations can affect the Stark splitting of the multiplets [29] as well as transition intensities [30]. These configurations have different influence on the lower and higher lying multiplets. This is mainly related to the energy gap between the multiplet and excited configuration. Within the J–O theory, excited configurations are considered to be completely degenerated and thus the above mentioned influence is not taken into account. The use of J–O theory for the description of transition intensities for Er^{3+} doped materials is typically successful [24–28]. This is due to the fact that multiplets of Er^{3+} ion are strongly "mixed" by the crystalline field and the difference in the action of excited configurations on different multiplets is near negligible. Indeed, the J-O theory allowed us to obtain low root-mean-square (rms) deviation between the experimental and calculated *f* values (rms dev. = 0.245).

PL spectra of the Er:YSGG crystal are shown in Fig. 3 (for excitation to the $^4I_{11/2}$ state by 962 nm radiation). Near-IR emissions at 0.95–1.05, 1.45–1.66 and 2.6–2.95 μm correspond to the transitions $^4I_{11/2} \rightarrow {}^4I_{15/2}$, $^4I_{13/2} \rightarrow {}^4I_{15/2}$ and $^4I_{11/2} \rightarrow {}^4I_{13/2}$, respectively. All visible emissions are due to up-conversion luminescence (UCL). The red emission band spanning from 640 to 690 nm and related to the transition $^4F_{9/2} \rightarrow {}^4I_{15/2}$ dominates in this spectrum. Green UCL (510–570 nm) from the closely located and thermalized states, $^2H_{11/2}$ and $^4S_{3/2}$, is much weaker. The ratio of the integrated intensities of these bands (R/G) is 3.1. Near-IR UCL at 780–870 nm is due to the $^4I_{9/2} \rightarrow {}^4I_{15/2}$ and $^4S_{3/2} \rightarrow {}^4I_{13/2}$ transitions. In the blue-violet region, very weak emissions at ~ 415 and 450 nm occur from the higher-lying $^2H_{9/2}$ and $^4F_{3/2}$+$^4F_{5/2}$ excited states, respectively.

In Fig. 4, log-log plots for the UCL intensity, I_{UCL}, vs. the excitation power density *W* are shown. UCL is a non-linear process, so typically $I_{UCL} \sim W^n$ (the so-called power law). The parameter *n* indicates the number of pump photons involved in the UCL mechanism. On a log-log scale, *n* corresponds to the slope of the above mentioned dependence. First we consider the case of low power densities (< 0.2 kW/cm^2). For green emissions that occur from the $^2H_{11/2}$ and $^4S_{3/2}$ states, *n* = 1.8 (542 nm) and 2.0 (557 nm) which means that two pump photons are required to populate the above mentioned states. A pump wavelength of ~962 nm corresponds to the ground-state absorption (GSA) $^4I_{15/2} \rightarrow {}^4I_{11/2}$. Further excitation is typically due to an excited state absorption (ESA) $^4I_{11/2} \rightarrow {}^4F_{7/2}$ or energy-transfer up-conversion (ETU) for adjacent Er^{3+} ions, $^4I_{11/2}$+ $^4I_{11/2} \rightarrow {}^4I_{15/2}$ + $^4F_{7/2}$. Taking into account fast non-radiative relaxation from the $^4F_{7/2}$ state, both $^2H_{11/2}$ and $^4S_{3/2}$ states are normally populated in a scheme that requires 2 pump photons that is in agreement with Fig. 4(a). For near-IR UCL at 857 nm, also occurring from the $^4S_{3/2}$ state, *n* = 1.9.

For red emission at 672 nm, *n* = 2.0. Population of the $^4F_{9/2}$ state, which is responsible for this emission, normally occurs in three steps. These are GSA, followed by a non-radiative relaxation to the intermediate $^4I_{13/2}$ level and second intense ESA channel $^4I_{13/2} \rightarrow {}^4F_{9/2}$. For crystals with a high Er content like in our case, there is an additional mechanism that allows for further enhancement of the excitation efficiency, namely cross-relaxation (CR). First intense CR scheme is $^4F_{7/2}$ + $^4I_{15/2} \rightarrow {}^4F_{9/2}$ + $^4I_{13/2}$ that raises red UCL. Second relevant CR scheme is $^4S_{3/2}$,$^2H_{11/2}$ + $^4I_{15/2} \rightarrow {}^4I_{9/2}$ + $^4I_{13/2}$ that depopulates thermalized $^4S_{3/2}$,$^2H_{11/2}$ states responsible for green emission. Increase of Er doping leads to a decrease of average inter-ionic distances and, hence, to a fast enhancement of the CR efficiency. In contrast, ESA process is not significantly affected by Er doping level. Thus, red UCL is

enhanced much stronger as compared with the green UCL from the thermalized $^2H_{11/2}$ + $^4S_{3/2}$ states that results in R/G ratio being > 1 for highly Er-doped crystals. Indeed, for 38 at. % Er:YSGG, R/G = 3.1 as mentioned above.

The reduced value of n for red UCL at high excitation power densities >0.2 kW/cm^2 (n ~1.1) is related to the competition of a linear decay (near-IR luminescence around 1.54 μm from the $^4I_{13/2}$ state) and upconversion itself (due to ESA from the $^4I_{13/2}$ state) in the depletion of the intermediate excited state, $^4I_{13/2}$. It was shown [31] that for strong UCL, n is typically <2 and can even approach 1. This prediction agrees with our results shown in Fig. 4. Similar behavior is observed for green and near-IR UCL.

Using the parameters presented in Table 2, we calculated line strengths $S_{ED}(JJ')$ for spontaneous radiative transitions from all excited states of the Er^{3+} ion from $^4I_{13/2}$ to $^2H_{9/2}$. On the basis of $S_{ED}(JJ')$ values, the corresponding probabilities of these transitions $A_{ED}(JJ')$ were determined as:

$$A_{ED}(JJ') = \frac{64\pi^4}{3h(2J+1)\bar{\lambda}^3} n\left(\frac{n^2+2}{3}\right)^2 S_{ED}(JJ') . \quad (4)$$

The total probabilities, $A(JJ') = A_{ED}(JJ') + A_{MD}(JJ')$, were then determined by adding MD contributions determined separately. Radiative lifetimes of the excited-states τ_{rad} and luminescence branching ratios $B(JJ')$ were then determined as:

$$\tau_{rad} = \frac{1}{\sum_{J'} A(JJ')} , \quad (5a)$$

$$B(JJ') = \frac{A(JJ')}{\sum_{J'} A(JJ')} . \quad (5b)$$

Luminescence branching ratios $B(JJ')$ for spontaneous radiative transitions from the $^4I_{13/2}$...$^2H_{9/2}$ states of Er^{3+} ions in YSGG determined with the J–O theory are shown in Table 3. For transitions from the $^4I_{11/2}$ state that is the upper-laser level for ~3 μm Erbium lasers, $B(^4I_{11/2} \rightarrow {}^4I_{15/2})$ = 74.6% and B ($^4I_{11/2} \rightarrow {}^4I_{13/2}$) =25.4%. In Table 4, we compared these values with the ones reported previously for Er:YSGG and different well-known Er-doped laser materials. The values calculated by us agree well with the ones reported for 30 at.% Er:YSGG in [16], namely 72.6% and 27.4%, respectively. They are also in agreement with ones presented for cubic garnets, Er:YAG, LuAG [24], GGG and GSGG [32].

Radiative lifetimes τ_{rad} for the $^4I_{13/2}$...$^2H_{9/2}$ excited-states of Er^{3+} ions in YSGG crystal are summarized in Table 5. Relatively good agreement of all τ_{rad} values is observed with the previous report for 30 at.% Er:YSGG [16]. For $^4I_{13/2}$ and $^4I_{11/2}$ states which are interesting for laser applications, τ_{rad} is 7.73 and 9.75 ms, respectively (as determined with the J–O theory). This is close to the result of [16] also obtained with the J–O theory, namely 6.62 and 8.87 ms, respectively. In Table 6, we compared radiative lifetimes of the $^4I_{13/2}$ and $^4I_{11/2}$ states for different Er^{3+}-doped crystals reported so far. A relatively good agreement of results for the $^4I_{13/2}$ state is observed. In contrast, for the $^4I_{11/2}$ state, the value of τ_{rad} for the Er:YSGG crystal is longer than ones determined for cubic Er-doped garnets (5–8 ms) [17,24] that highlights its potential for 3 μm laser operation.

The knowledge of radiative lifetimes τ_{rad} for the $^4I_{13/2}$ and $^4I_{11/2}$ states allows for determination of stimulated-emission cross-sections, σ_{SE}, for laser-active transitions $^4I_{13/2} \rightarrow {}^4I_{15/2}$ (lasing at ~1.5 μm) and $^4I_{11/2} \rightarrow {}^4I_{13/2}$ (at ~3 μm). In both cases, the Füchtbauer–Ladenburg (F-L) equation [35] was used:

$$\sigma_{SE}(\lambda) = \frac{\lambda^5}{8\pi n^2 \tau_{rad} c} \frac{3W(\lambda)}{\int \lambda W(\lambda) d\lambda} . \quad (6)$$

Here $W(\lambda)$ is the measured spectral power density of luminescence. In addition, for the $^4I_{13/2} \rightarrow {}^4I_{15/2}$ transition, we used the reciprocity method:

$$\sigma_{SE}(\lambda) = \sigma_{abs}(\lambda) \frac{Z_1}{Z_2} \exp\left(-\frac{hc/\lambda - E_{ZL}}{kT}\right) , \quad (7)$$

where Z_1 and Z_2 are the lower and upper manifold partition functions, respectively, E_{ZL} is the energy corresponding to the zero phonon line, k is the Boltzmann constant and T is the crystal temperature (room-temperature). Partition functions are determined as:

$$Z_m = \sum_k g_k^m \exp(-E_k^m/kT), \tag{8}$$

where m = 1, 2; $g^m{}_k$ is the degeneration of the sublevel having the number k and the energy $E^m{}_k$ measured from the lower sublevel of the corresponding multiplet. The energies of sublevels for the $^4I_{13/2}$ and $^4I_{15/2}$ multiplets for Er:YSGG crystal were taken from [15]. Calculation of σ_{SE} with the reciprocity method is beneficial as it does not require the information about the radiative lifetime τ_{rad} of the emitting state as well as direct measurement of the emission spectrum that can be affected by the reabsorption loss. There exists third possibility for the calculation of σ_{SE} values, the so-called modified reciprocity method [36]:

$$\sigma_{SE}(\lambda) = \frac{3\exp(-hc/(kT\lambda))}{8\pi n^2 \tau_{rad} c \int \lambda^{-4} \sigma_{abs}(\lambda) \exp(-hc/(kT\lambda)) d\lambda} \sigma_{abs}(\lambda). \tag{9}$$

Modified reciprocity method does not refer to the emission spectrum $W(\lambda)$ but it requires the data about τ_{rad} value. Thus, a simultaneous use of Eqs. (7) and (9) can result in an estimation of the radiative lifetime of the emitting state that is the $^4I_{13/2}$ state in our case.

The results for σ_{SE} are shown in Fig. 5. For the $^4I_{13/2} \rightarrow {}^4I_{15/2}$ transition, the use of reciprocity method corresponds to a better resolution of spectral features as compared with the F–L equation, partially referred to a better spectral resolution used in the absorption measurements and partially to the reabsorption losses that are strong for highly doped 38 at.% Er:YSGG crystals. The maximum stimulated-emission cross-section σ_{SE} is 1.20×10^{-20} cm^2 at 1532.8 nm. Estimation of the radiative lifetime τ_{rad} of the $^4I_{13/2}$ state with the modified reciprocity method yields the value of 5.5±0.5 ms that is shorter than one determined from the J–O modeling, 7.73 ms. This effect was previously observed in [32]. It can be explained as following. In the J–O theory, it is assumed that all the crystal field levels of each multiplet are equally populated. For the case of Er:YSGG crystal, the $^4I_{15/2}$ ground state is split into two groups of four levels separated by ~400 cm^{-1} [15]. Thus, the transitions from the four lower $^4I_{15/2}$ sub-levels to the $^4I_{11/2}$ and $^4I_{13/2}$ states are much stronger than they are from the upper four sub-levels. Since the lower group of levels is predominantly populated at room temperature, this splitting leads to an enhancement of the observed oscillator strength and therefore slight underestimate of the Judd-Ofelt radiative lifetime.

For laser applications, a useful parameter is also the gain cross-section, σ_g:

$$\sigma_g(\lambda) = \beta\sigma_{SE}(\lambda) - (1-\beta)\sigma_{abs}(\lambda), \tag{10}$$

where β is the inversion ratio, $\beta = N_2/N_0$ where N_2 and N_0 are the numbers of ions in the upper laser level and overall number of ions, respectively. The gain spectra for the Er:YSGG crystal for β <0.5 are shown in Fig. 5(b). In accordance with this plot, the dominant wavelength in the Er:YSGG laser working on the $^4I_{13/2} \rightarrow {}^4I_{15/2}$ transition will be at ~1644 nm. This is in agreement with the report on an Er:YSGG inband-pumped laser emitting at 1643 nm [37]. For real ~1.5 μm laser applications, concentration of Er^{3+} ions of <1 at.% should be selected to avoid the detrimental influence of strong up-conversion.

For the $^4I_{11/2} \rightarrow {}^4I_{13/2}$ channel, the maximum stimulated-emission cross-section is 0.43×10^{-20} cm^2 at 2797.1 nm, Fig. 5(c). This emission channel is free of reabsorption losses, so one can expect generation at this wavelength in an Er:YSGG laser.

Peak stimulated-emission cross-sections σ_{SE} for the $^4I_{13/2} \rightarrow {}^4I_{15/2}$ and $^4I_{11/2} \rightarrow {}^4I_{13/2}$ transitions of Er^{3+} ions for Er:YSGG and several Er^{3+}-doped crystals are compared in Table 7. It should be noted that σ_{SE} *spectrum* was never reported for the $^4I_{11/2} \rightarrow {}^4I_{13/2}$ transition of Er^{3+} ions in the YSGG crystal. Previously for the calculation of peak σ_{SE} value corresponding to this transition, lifetime of the $^4I_{11/2}$ upper laser level reported by Dinerman, τ_{exp}=3.4 ms [2], was used. This led to the overestimation of the σ_{SE} value that was typically considered to be ~2.8×10^{-20} cm^2. However, as in [2] τ_{exp} was determined directly from the PL decay curves for a highly-doped (30 at.% Er) crystal, it was much shorter

than the radiative lifetime, namely 9.75 ms as determined in the present paper from the J–O modeling. Similar situation for different Er-doped crystals is addressed in details in [32]. For the $^4I_{13/2} \rightarrow {}^4I_{15/2}$ transition, stimulated-emission and gain cross-sections spectra were also not reported for Er:YSGG crystal. However, the obtained peak σ_{SE} values for this transition are in accordance with the ones reported previously for different Er-doped materials, see Table 7.

The measured decay curves for the luminescence from the five lowest excited-states of Er^{3+} ions in YSGG are shown in Fig. 6 ($^4S_{3/2}$ and $^2H_{11/2}$ levels are treated as a single, thermally coupled level). Relatively high Er concentration should lead to significant concentration quenching and a high rate of non-radiative relaxation in the Er:YSGG crystal. Thus, shortening of the measured lifetime, τ_{exp}, as compared with the radiative one, τ_{rad}, is expected for all excited-states of Er^{3+} ions. The measured decay times τ_{exp} of the luminescence from the $^4I_{13/2}$ and $^4I_{11/2}$ states are 2.24 and 1.3 ms, respectively (compare with the corresponding radiative lifetimes, 7.73 and 9.75 ms as determined from the J–O modeling). The value of $\tau_{exp}(^4I_{13/2})$ obtained in the present paper for 38 at.% Er:YSGG crystal is shorter than the value reported in [2] for 30 at.% Er doped crystal, namely 3.2 ms. For the $^4I_{9/2} - {}^2H_{11/2}$ states, the measured lifetimes are on the order of a few μs (cf. Table 5). By comparing τ_{rad} for the $^4F_{9/2}$ state (responsible for red emission) and the thermalized $^4S_{3/2}+{}^2H_{11/2}$ states (responsible for green UCL), the prevalence of red emission in the UCL can be explained. Indeed, $\tau_{rad}(F_{9/2}) = 10.2$ μs which is nearly 25 times longer than for the $^4S_{3/2}$ and $^2H_{11/2}$ states. In addition, the lifetime of the $^4I_{11/2}$ state is shorter than that of the $^4I_{13/2}$ state, so the ESA process ($^4I_{13/2} \rightarrow {}^4F_{9/2}$) that populates the $^4F_{9/2}$ level responsible for red emission will be stronger.

By comparing radiative lifetimes of the excited states [$\tau_{rad} = \Sigma_{J'}A(JJ')$] and measured decay times for the luminescence from these states, τ_{exp}, we estimated the nonradiative decay-rate constants, $A_{NR} = (1/\tau_{exp}) - \Sigma_{J'}A(JJ')$, see Table 8. The value of A_{NR} is related to the energy gap ΔE between the considered state and the lower-lying state by the equation [42]:

$$A_{NR} = Ce^{-\alpha\Delta E}, \qquad (11)$$

where C and α are the constants characteristic of the host material. Eq. (11) is applicable for a constant temperature and concentration of active ions.

In Fig. 6(d), we plotted the obtained values of A_{NR} vs. the minimum energy gap ΔE_{min} between the excited-states calculated from the known structure of energy levels of Er^{3+} ions in the YSGG crystal. In a semi-log scale, this dependence was fitted by a linear law yielding $C = 3.4\times10^7$ s^{-1} and $\alpha = 2.0\times10^{-3}$ cm constants. The agreement between the calculated A_{NR} values and the best-fitting curve is satisfactory for the $^4I_{13/2}$, $^4I_{9/2}$, $^4F_{9/2}$ and $^4S_{3/2} + {}^2H_{11/2}$ states, while for the $^4I_{11/2}$ state the calculated A_{NR} value (666.6 s^{-1}) is one order of magnitude lower than one predicted from the linear fit (~8×10^4 s^{-1}). Thus, simple model described by Eq. (11) that is typically used for the description of nonradiative decay in Er^{3+}-doped materials with a relatively low Er^{3+} concentrations [43], predicts even stronger shortening of the luminescence lifetime of the $^4I_{11/2}$ state for Er:YSGG crystal. However, particularly long τ_{exp} value for this state makes Er:YSGG crystal attractive for laser operation on the $^4I_{11/2} \rightarrow {}^4I_{13/2}$ transition (i.e., as compared with Er:YAG).

The deviation of the experimental points on A_{NR} from the linear law is attributed to a very high concentration of Er^{3+} ions that could generate more complicated dependence between A_{NR} and ΔE. Indeed, the considered N_{Er} value (4.82×10^{21} at/cm^3) should be compared with the so-called quenching concentration N_q that corresponds to a reduction of the luminescence lifetime τ_{exp} with respect to the radiative one τ_{rad} by a factor of 2, $\tau_{exp} = \tau_{rad}/[1+(N_{Er}/N_q)^2]$ [44]. For Er^{3+} ions in YAG, N_q ~3×10^{21} at/cm^3 [45] (for the Er^{3+}:YSGG crystal, these data are not presented in the literature).

More significant shortening of τ_{exp} with respect to τ_{rad} for the $^4I_{11/2}$ state as compared with the $^4I_{13/2}$ state can be understood with Eq. (11) and the values of energy gaps ΔE_{min} for these states that are 3372 and 6370 cm^{-1}, respectively. If considering multi-phonon mechanism of the non-radiative decay, this means that ~5 and 9 phonons are required to depopulate theses states (here we consider the maximum vibrational frequency of YSGG, ν_{max} = 752 cm^{-1} [46]). Thus, for the $^4I_{11/2}$ state this process should have much higher probability. Another mechanism of shortening of the τ_{exp} value can be en-

ergy-transfer to the impurities ions that in enhanced with the increase of the Er^{3+} concentration [45]. The probability of this energy-transfer can be different for the $^4I_{11/2}$ and $^4I_{13/2}$ states depending on if they are resonant in energy to the impurity states; in addition, this process is strongly dependent on the growth method and particular composition of the considered sample [45].

4. Conclusions

We report on a comprehensive spectroscopic study of a highly-doped 38 at.% Er:YSGG crystal. Optical absorption and luminescence of Er^{3+} ions is studied. The maximum absorption cross-section for the $^4I_{15/2} \rightarrow {}^4I_{11/2}$ transition is $\sigma_{abs} = 0.46\times10^{-20}$ at 965.8 nm. Radiative lifetimes of all excited states of the Er^{3+} ion from $^4I_{13/2}$ to $^2H_{9/2}$, branching ratios and probabilities of radiative transitions from these states are determined using the Judd-Ofelt theory. Radiative lifetimes of the $^4I_{13/2}$ and $^4I_{11/2}$ excited states for Er^{3+} ions in YSGG crystal are 7.73 ms and 9.75 ms, respectively. Using these relevant spectroscopic data, stimulated-emission cross-section spectra are evaluated for ~1.5 μm ($^4I_{13/2} \rightarrow {}^4I_{15/2}$) and 3 μm ($^4I_{11/2} \rightarrow {}^4I_{13/2}$) transitions. For the $^4I_{11/2} \rightarrow {}^4I_{13/2}$ channel, the maximum stimulated-emission cross-section is 0.43×10^{-20} cm^2 at 2797.1 nm. The role of non-radiative relaxation on the shortening of luminescence lifetimes of lower excited-states of Er^{3+} is discussed.

References

1. H. Stange, K. Petermann, G. Huber, E. W. Duczynski, Appl. Phys. B 49 (1989) 269-273.
2. B. J. Dinerman, P. F. Moulton, Opt. Lett. 19 (1994) 1143-1145.
3. J.S. Liu, J.J. Liu, Y. Tang, Laser Phys. 18 (2008) 1124-1127.
4. A. Aubourg, J. Didierjean, N. Aubry, F. Balembois, P. Georges, Opt. Lett. 38 (2013) 938-940.
5. H. Jelinkova, T. Dostalova, K. Hamal, O. Krejsa, J. Kubelka, S. Prochazka, Laser Phys. 8 (1998) 176-181.
6. A. Zajac, M. Skorczakowski, J. Swiderski, P. Nyga, Opt. Express 12 (2004) 5125-5130.
7. M. Pollnau, W. Luthy, H.P. Weber, "*Influence of normal and inverse upconversion processes on the continuous wave operation of the Er^{3+} 3 μm crystal laser*", Vol. 20 of OSA Proceedings Series (Optical Society of America, 1994), P. EL5.
8. S. Georgescu, O. Toma, IEEE J. Selected Top. Quantum Electron. 11 (2005) 682-689.
9. V. Lupei, S. Georgescu, V. Florea, IEEE J. Quantum Electron. 29 (1993) 426-434.
10. S. Georgescu, O. Toma, H. Totia, IEEE J. Quantum Electron. 39 (2003) 722-732.
11. E. A. Arbabzadah, C. C. Phillips, M. J. Damzen, Appl. Phys. B 111 (2013) 333-339.
12. E. A. Arbabzadah, S. Chard, H. Amrania, C. C. Phillips, M. J. Damzen, Opt. Exp. 19 (2011) 25860-25865.
13. P. F. Moulton, J. G. Manni, and G. A. Rines, IEEE J. Quantum Electron. 24 (1998) 960-973.
14. E. Zharikov, N.N. Il'ichev, S.P. Kalitin, V.V. Laptev, A.A. Malyutin, V.V. Osiko, P.P. Pashinin, A.M. Prokhorov, Z.V. Saidov, V.A. Smirnov, A.F. Umyskov, I.A. Shcherbakov, Sov. J. Quantum Electron. 16 (1986) 635–639.
15. J.B. Gruber, J.R. Quagliano, M.F. Reid, F.S. Richardson, M.E. Hills, M.D. Seltzer, S.B. Stevens, C.A. Morrison, T.H. Allik, Phys. Rev. B 48 (1993) 15561-15573.
16. J. Su, C. Yang, Q. Li, Q. Zhang, J. Luo, J. Lumin. 130 (2010) 1546–1550.
17. D.K. Sardar, W.M. Bradley, J.J. Perez, J.B. Gruber, B. Zandi, J.A. Hutchinson, C.W. Trussell, M.R. Kokta, J. Appl. Phys. 93 (2003) 2602.
18. X.S. Chen, J. Collins, B. DiBartolo, B. Bowlby, B. Dinerman, D. Weyburne, J. Lumin. 72-74 (1997) 168.
19. X.S. Chen, T. Nguyen, Q. Luu, B. Dibartolo, J. Lumin. 83-84 (1999) 471.
20. Q.Y. Wang, S.Y. Zhang, Y.Q. Jia, J. Alloys & Cmpd. 202 (1993) 1.
R. Micheletti, P. Minguzzi, M. A. Noginov, M. Tonelli, J. Opt. Soc. Amer. B 11 (1994) 2095-2099.
21. B.R. Judd, Phys. Rev. 172 (1962) 750–761.
22. G.S. Ofelt, J. Chem. Phys. 37 (1962) 511–519.

23. E.V. Zharikov, V.F. Kitaeva, V.Y. Fedorovich, Sov. Phys. Solid State 31 (1989) 298–299.
24. A.A. Kaminski, A.G. Petrosyan, G.A. Denisenko, T.I. Butaeva, V.A. Fedorov, S.E. Sarkisov, Phys. Stat. Sol. (a) 71 (1982) 291.
25. I.A. Belova, F.A. Bolshchikov, Yu.K. Voronko, A.V. Malov, A.V. Popov, P.A. Ryabochkina, A.A. Sobol, S.N. Ushakov, Phys. Solid State 50 (2008) 1611.
26. W.F. Krupke, M.D. Shinn, J.E. Marion, J. Opt. Soc. Am. B 3 (1986) 102.
27. M.J. Weber, Phys. Rev. 171 (1968) 283.
28. A.A. Kaminski, V.S. Mironov, A.A. Kornienko, S.N. Bagaev, G. Boulon, A. Brenier, B. Di Bartolo, Phys. Stat. Sol. (a) 151 (1995) 231.
29. P.A. Tanner, C.S.K. Mak, M.D. Faucher, W.M. Kwok, D.L. Phillips, V. Mikhailik, Phys. Rev. B 67 (2003) 115102.
30. E.B. Dunina, A.A. Kornienko, L.A. Fomicheva, Cent. Eur. J. Phys. 6 (2008) 407–414.
31. M. Pollnau, D.R. Gamelin, S.R. Lüthi, H.U. Güdel, M.P. Hehlen, Phys. Rev. B 61 (2000) 3337 – 3346.
32. S.A. Payne, L.K. Smith, W.F. Krupke, J. Appl. Phys. 77 (1995) 4274.
33. M.J. Weber, Phys. Rev. 157 (1967) 262.
34. M. Pollnau, R. Spring, Ch. Ghisler, S. Wittwer, W. Luthy, H.P. Weber, IEEE J. Quantum Electron. 32 (1996) 657.
35. B.F. Aull, H.P. Jenssen, IEEE J. Quantum Electron. 18 (1982) 925–930.
36. A.S. Yasyukevich, V.G. Shcherbitskii, V.E. Kisel, A.V. Mandrik, N.V. Kuleshov, J. Appl. Spectr. 71 (2004) 202-208.
37. K. Spariosu, M. Birnbaum, M. Kokta, Appl. Opt. 34 (1995) 8272-8275.
38. M. Tikerpae, S.D. Jackson, T.A. King, J. Modern Opt. 45 (1998) 1269.
39. E.V. Zharikov, V.I. Zhekov, T.M. Murina, V.V. Osiko, M.L Timoshechkin, I.A. Shcherbakov, Sov. J. Quantum Electron. 7 (1977) 117.
40. D Koetke, G. Huber, Appl. Phys. B 61 (1995) 151.
41. T. Schweizer, T. Jensen, E. Heumann, G. Huber, Opt. Commun. 118 (1995) 557.
42. N. Yamada, S. Shionoya, T. Kushida, J. Phys. Soc. Jpn. 32 (1972) 1577–1586.
43. L. Agazzi, K. Wörhoff, A. Kahn, M. Fechner, G. Huber, M. Pollnau, J. Opt. Soc. Am. B 30 (2013) 663-677.
44. H. Higuchi, M. Takahashi, Y. Kawamoto, K. Kadono, T. Ohtsuki, N. Peyghambarian, N. Kitamura, J. Appl. Phys. 83 (1998) 19-27.
45. S. Georgescu, V. Lupei, A. Lupei, V. I. Zhekov, T. M. Murina, M. I. Studenikin, Opt. Commun. 81 (1991) 186-192.
46. D. Chiriu, P.C. Ricci, C.M. Carbonaro, A. Anedda, M. Aburish-Hmidat, A. Grosu, P.G. Lorrai, E. Fortin, J. Appl. Phys. 100 (2006) 033101.

List of figure captions

Figure 1 Erbium energy level diagram.

Figure 2 Absorption cross-section spectra for 38 at.% Er:YSGG crystal.

Figure 3 (a) Near-IR luminescence from 38 at.% Er:YSGG crystal, bands at 0.95–1.7 μm and 2.6–3 μm are not in scale; (b) up-conversion luminescence (UCL) from this crystal, excitation wavelength is 962 nm.

Figure 4 Dependence of the UCL intensity on the excitation power density for 38 at.% Er:YSGG, *points* are the experimental data, *lines* are their fitting for the slope (*n*) calculation.

Figure 5 Stimulated-emission cross-section σ_{SE} spectra for the $^4I_{13/2} \rightarrow {}^4I_{15/2}$ (a) and $^4I_{11/2} \rightarrow {}^4I_{13/2}$ (c) transitions of Er^{3+} ions in Er:YSGG crystal, as calculated with the reciprocity, Eq. (7) and Füchtbauer–Ladenburg (F–L) methods, Eq. (6); gain cross-section, $\sigma_g = \beta\sigma_{SE}-(1-\beta)\sigma_{abs}$, spectrum for the $^4I_{13/2} \rightarrow {}^4I_{15/2}$ transition (b), β is the inversion ratio.

Figure 6 Luminescence decay curves for emissions from the $^4I_{13/2}$, $^4I_{11/2}$ (a), $^4I_{9/2}$ (b), $^4F_{9/2}$ and $^4S_{3/2}$ (c) excited-states of Er^{3+} ions in the 38 at.% Er:YSGG crystal under resonant excitation; (d) energy-gap dependence of the nonradiative decay-rate constants A_{NR} in 38 at.% Er:YSGG in a semi-log scale: *points* are the values determined with the measured luminescence lifetimes and the calculated radiative decay rate constants, *line* is the fit through these data with Eq. (11).